



Transition metal oxide nanostructures: premeditated fabrication and applications in electronic and photonic devices

Feiyu Diao¹ and Yiqian Wang^{1,*}

¹ College of Physics, Qingdao University, No. 308, Ningxia Road, Qingdao 266071, People's Republic of China

Received: 11 September 2017

Accepted: 22 November 2017

Published online:
27 November 2017

© Springer Science+Business Media, LLC, part of Springer Nature 2017

ABSTRACT

Transition metal oxide (TMO) nanomaterials possess both novel nanoeffects and excellent semiconductor properties that make them promising materials for electronics and photonics. Great expectations have been placed on TMO nanomaterials to deal with the global challenges in many fields, especially portable equipment and energy issues. In the last decades, extensive research work concentrated on the synthesis, microstructure, and macro-performance of TMO nanomaterials. A comprehensive understanding of both growth mechanism and underlying relationship between microstructure and physical properties can lead to performance enhancements of TMO nanomaterials in electronics and photonics, which in turn enables the fabrication TMO nanostructures based on anticipated design strategies. At present, TMO nanostructures do not satisfactorily meet the technical criteria for direct practical applications in electronics and photonics. In this paper, recent developments in synthesis, characterization, and prominent applications of TMO nanomaterials are reviewed from a structural perspective, which serves as a stepping stone to develop novel nanostructures with superior performances and provides a necessary guidance for transformation of scientific achievements into practical applications.

Introduction

Electronics and photonics use electrons and photons as main information carriers, which have always been hot research topics with numbered applications in people's daily life for hundreds of years. The thriving of portable intelligent electronic device boosts the development of components toward mini-

size and high performance. Particularly worth mentioning is the huge energy demands for massive production and the consequent environmental pollution [1]. A new opportunity to deal with these enormous challenges has been provided by nanomaterials, whose small sizes and high specific surface areas lead to their characteristic properties [2, 3]. A wide range of nanomaterials has been fabricated for

Address correspondence to E-mail: yqwang@qdu.edu.cn

their applications in novel electronic and photonic devices. For example, gold (Au) nanoparticles are used in biosensors due to their fast response [4]; graphene is very popular in various composite systems because of its unique frame structure and excellent conductivity [5]; metal chalcogenides present distinctive electronic and optical properties owing to the strong spin-orbital coupling [6]. Besides, transition metal oxide (TMO) is considered to be one of the most promising functional materials because of its unique components, in which the combination of positive metallic and negative oxygen ions exhibits various structures and suitable physical properties such as long-term environmental stability, wide bandgap and optically active electronic transition. The abundant mineral resources lay a solid foundation for environmentally friendly industrialization of TMO nanomaterials with low cost. Therefore, we focus on the development of TMO nanomaterials with different structures. Since the discovery of TiO₂-based dye-sensitized solar cells [7] and ZnO nanolasers [8], significant progress has been achieved regarding the synthesis, structural characterization, electronic and optical properties of TMO nanostructures, and their applications in nanodevices. Up to now, multifarious TMO nanostructures including quantum dots, nanoparticles, and one-dimensional (1D) and two-dimensional (2D) nanomaterials have been fabricated consecutively and have demonstrated various structure-related performances. For instance, quantum dots exhibit distinct quantum confinement effect; nanoparticles provide specific exposed surfaces which have different sensitivity to external stimuli; 1D and 2D nanomaterials demonstrate the ultrahigh carrier mobility by confining the migratory direction of charge carriers.

Promising application potentials of TMO nanomaterials are presented in photodetection, gas sensing, light emission, energy storage, and photocurrent generation [9–11]. Figure 1 shows the evolution of the yearly publications for several representative TMO nanostructures and their applications. It can be seen from Fig. 1a that the research about TMO nanostructures increases yearly, especially for ZnO. More attention has been paid on the applications of TMO nanostructures in electronic and photonic devices in the past 5 years, as shown in Fig. 1b. However, the application of TMO-based devices in practice is still far away, limited by controllable preparation techniques and deep understanding of growth

mechanisms involved in the synthesis of TMO nanomaterials. Thus, there are still many scientific challenges to overcome for exploiting the outstanding performances of TMO nanomaterials.

Our article will specifically focus on the fabrication techniques employed to synthesize TMO compounds, their structural characterization at an atomic scale, and their growth mechanisms. Recent application developments of TMO nanomaterials will be then reviewed for implementation in photoelectric devices, energy harvest and storage, and the development of ecological products.

Fabrication of TMO nanostructures

The physical properties of TMO materials are strongly connected with their morphology. This motivates the development of various preparation techniques, which can drastically affect both the dimensions and the nature of nanomaterials. To achieve the goals of manufacturing nanostructures based on anticipated design strategies economically, it is essential to investigate their growth mechanism. A comprehensive understanding will offer the intrinsic guidance at an atomic or molecular scale for monitoring and optimizing their fabrication. Such investigations require the aid of transmission electron microscopy (TEM), which is suitable for the microstructural characterization. This powerful experimental technique provides information regarding the overall particle size, morphology and inner atomic structure of TMO nanomaterials, which is crucial for the optimization of their synthesis process. In this section, we present the commonly used synthetic methods and associated growth mechanisms for various TMO nanostructures with different dimensions.

0D nanostructures (nanoparticles)

Zero-dimensional (0D) nanostructures are usually related to particles with diameters of a few nanometers, which can provide specific exposed surfaces. Until now, nanoparticles with different morphologies of sphere, cube, octahedron, dodecahedron, and so on have been synthesized by various preparation methods. Among numerous techniques, hydrothermal synthesis and electrochemical deposition are most widely used. Hydrothermal synthesis is

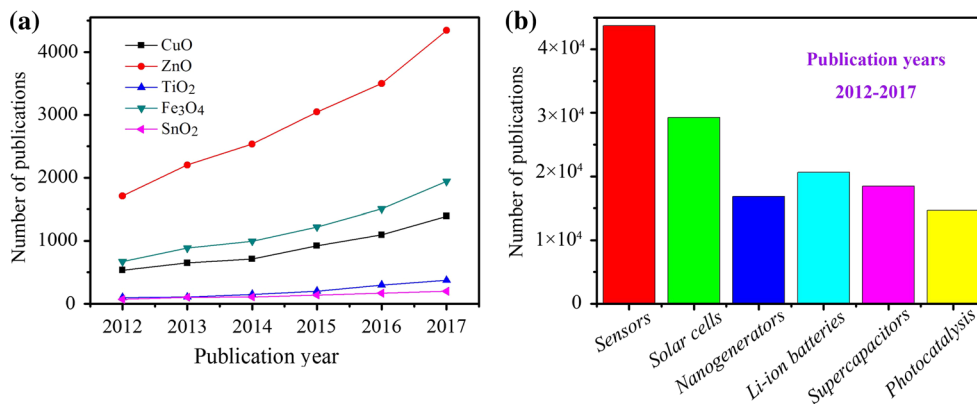


Figure 1 Research focus of **a** representative TMO nanomaterials and **b** their applications in the past 5 years.

suitable for preparation of most TMO nanostructures [12–15]. Massive alternative surfactants make it possible to boom the morphologies of TMO nanostructures. Recently, our group has successfully synthesized SnO₂ nanostructures with different morphologies including hierarchical nanorods, nanododecahedra, and nanoparticles using different surfactants in one-step hydrothermal process [16]. Hierarchical nanorods are obtained by adding NaOH aqueous solution into tin (Sn)-based solution, while hierarchical nanododecahedra and nanoparticles are produced by adding organic surfactants of sodium alginate or benzimidazole. Figure 2 shows typical TEM images of hierarchical SnO₂ nanorods, nanododecahedra, and nanoparticles, including bright-field (BF) image, selected-area electron diffraction (SAED) pattern and high-resolution TEM (HRTEM) image. From Fig. 2, it can be seen that the hierarchical nanododecahedra and nanoparticles are much smaller than nanorods, indicating that addition of organic surfactants can reduce the particle size and tailor exposed surfaces. Nevertheless, the growth mechanism for hydrothermal synthesis remains to be comprehensively understood due to the complex and volatile additives.

Electrochemical deposition is an effective method to tailor TMO nanostructures by adjusting experimental conditions. Using this method, Choi et al. [17, 18] have achieved a series of morphology transformation of Cu₂O crystals. Scanning electron microscope (SEM) images in Fig. 3 show the transformation of cubic Cu₂O crystals. A basic crystal shape is determined by two growth processes, habit formation, and branching growth. Crystal habit is determined by the relative order of surface energies

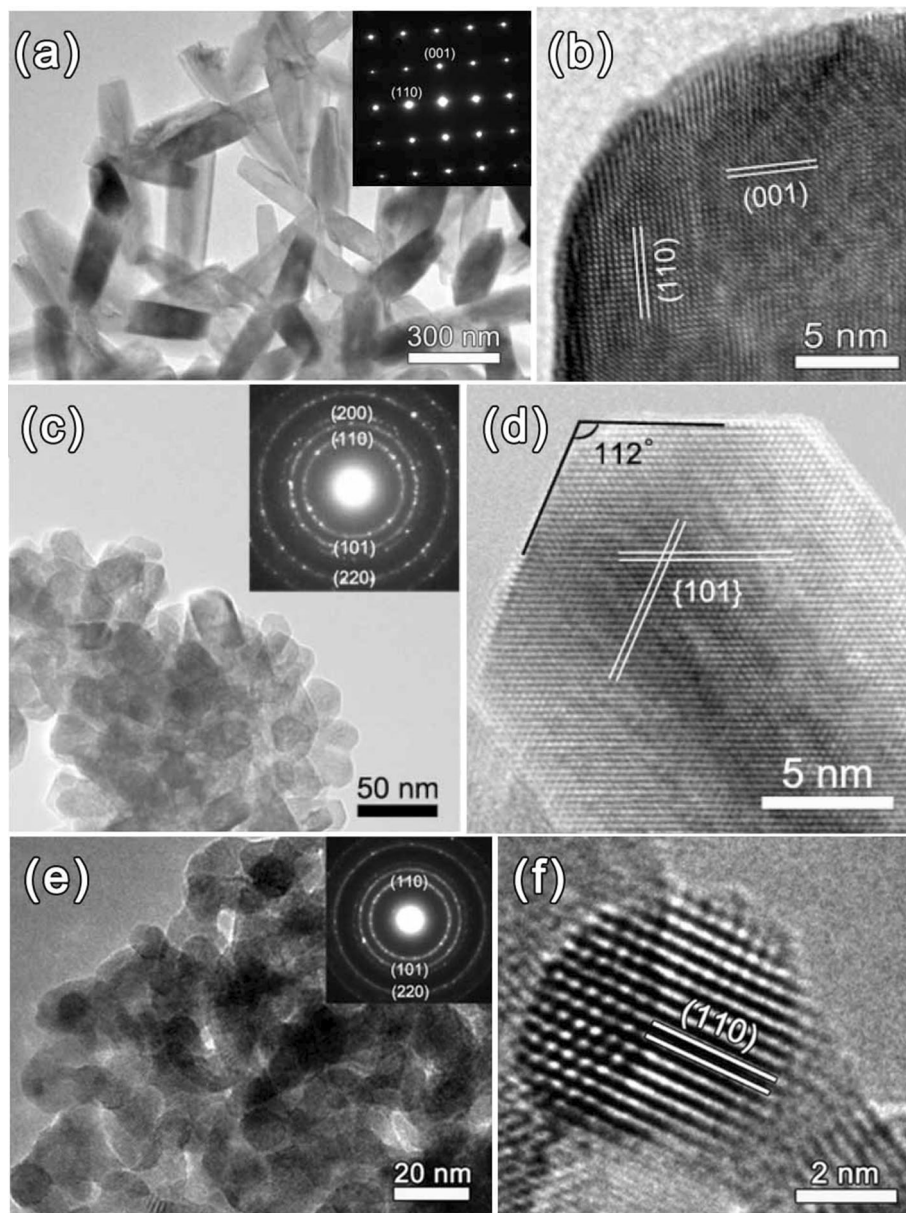
of different crystallographic planes of a crystal, and branching growth is created by a diffusion effect. The capping agents (molecules or ions) during the growth of nanoparticles can be used to tailor the ratio between the growth rates along the $\langle 100 \rangle$ and $\langle 111 \rangle$ directions to selectively control the formation of exposed surfaces. The results obtained by Choi et al. [17, 18] have demonstrated that the methodical and simultaneous tuning of the habit and the degree of branching of Cu₂O crystals can be realized by manipulating the key conditions that control shape-guiding processes.

Based on the mechanism mentioned above, our group [19] synthesized uniform Cu₂O nanooctahedra on aluminum (Al) foils by electrochemical deposition. TEM investigation in Fig. 4 illustrates that the growth direction of Cu₂O nanocrystal is along $\langle 001 \rangle$. On this basis, a facile electrodeless deposition method [20] was developed for the preparation of Cu₂O nanooctahedra by immersing metal substrate into a basic solution consisting of CuSO₄ and lactic acid. The formation mechanism of Cu₂O nanooctahedra is proposed in Fig. 5, in which the synergistic effects of the reduction of Cu²⁺ by metal substrates and surface selective adsorption of lactic acid play a critical role.

1D nanostructures

One-dimensional nanostructures have diverse forms such as nanowires (NWs), nanotubes, nanobelts, and nanofibers [21–24]. Enormous effort has been made to synthesize 1D TMO nanostructures. Based on different growing environments, these synthetic methods can be divided into two categories: vapor-phase growth and liquid-phase growth. As suggested by

Figure 2 Typical BF TEM images of **a** hierarchical nanorods, **c** nanododecahedra, and **e** nanoparticles. Insets are corresponding SAED patterns. Typical HRTEM images of **b** hierarchical nanorods, **d** nanododecahedra, and **f** nanoparticles. Reprinted with permission from ref. [16]. Copyright 2016 Elsevier.



the names, 1D nanostructures are fabricated in atmosphere (usually in oxygen) for vapor-phase growth and in solution for liquid-phase growth system. Massive 1D TMO nanostructures can be synthesized by either vapor-phase growth or liquid-phase growth technique. Vapor-phase growth technique has stringent requirements on reaction temperature and experimental equipment, whereas liquid-phase growth technique at moderate temperature helps to reduce costs and simplify experimental operations.

Vapor-phase growth

Vapor-phase growth techniques include direct physical deposition and chemical deposition. Physical vapor deposition (PVD) is one of the most important physical deposition techniques, in which the surface atoms of bulk TMO sublime into TMO vapor, and subsequently the TMO vapor condenses into 1D TMO nanostructures on substrates. Moreover, 1D TMO nanostructures can be easily synthesized using chemical deposition techniques. Chemical vapor deposition (CVD) techniques are widely applied in the semiconductor industry

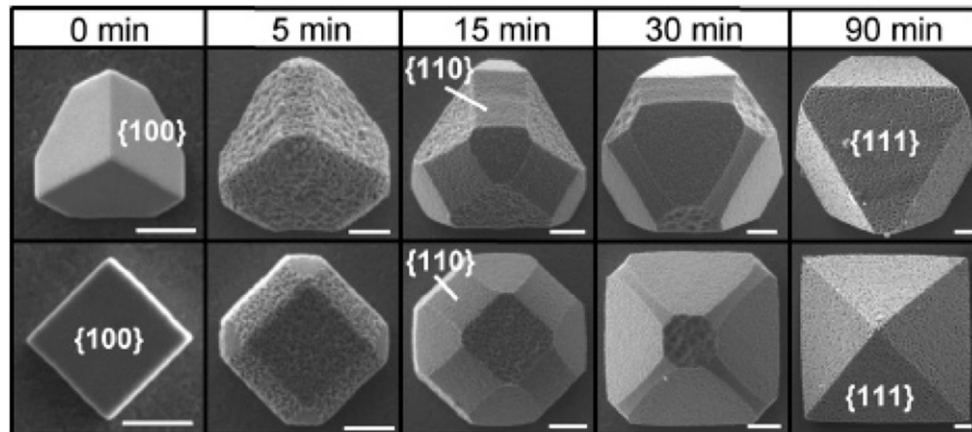


Figure 3 SEM images showing the transformation of cubic Cu_2O crystals. Top: view along the $\langle 111 \rangle$ direction; Bottom: $\langle 100 \rangle$ direction. Scale bar = 1 μm . Reprinted with permission from ref. [17]. Copyright 2006 American Chemical Society.

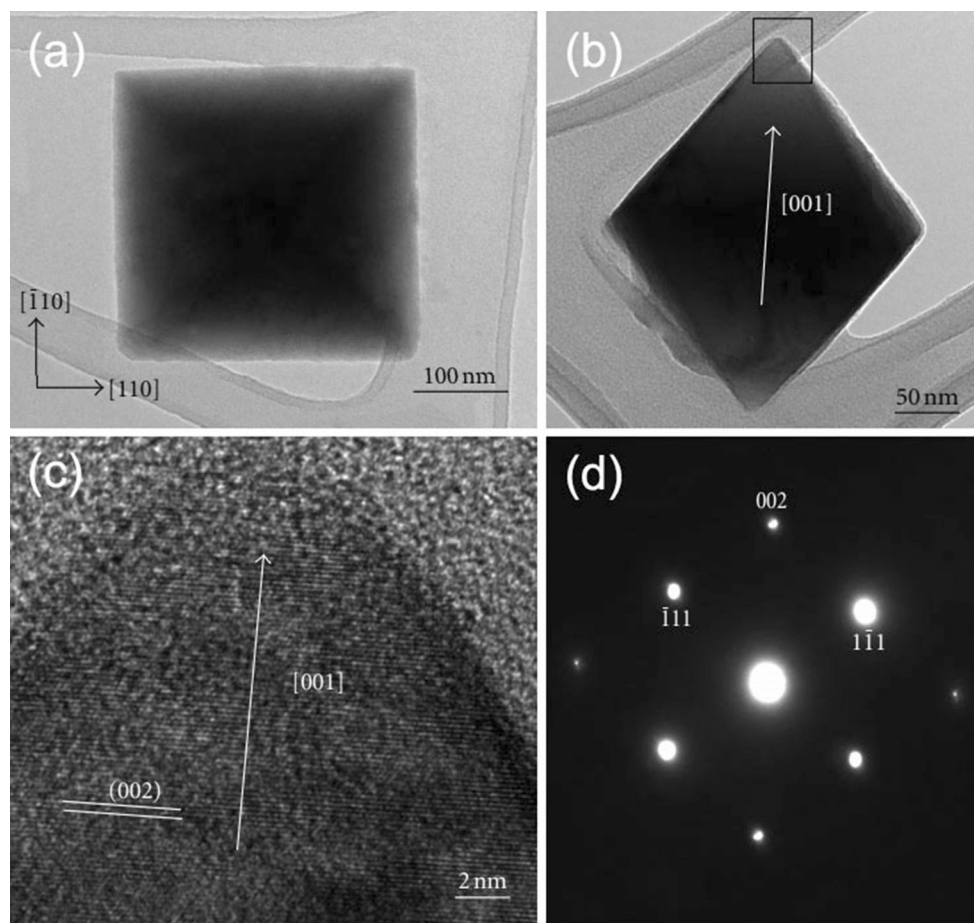
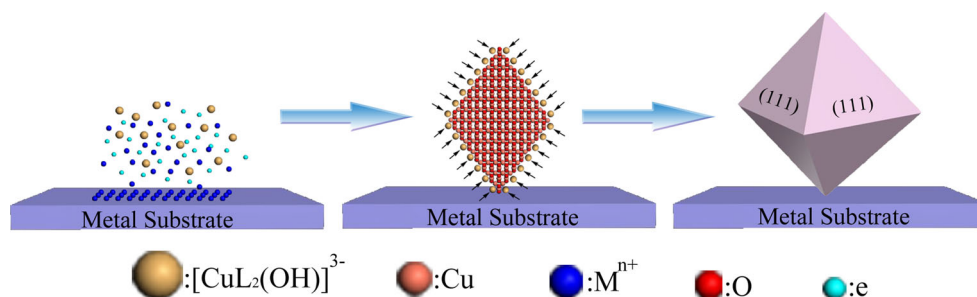


Figure 4 TEM images of individual Cu_2O octahedron viewed from **a** the top and **b** the side. **c** Typical HRTEM image of the region enclosed by a square in **b**. **d** Corresponding SAED pattern. Reprinted with permission from ref. [19]. Copyright 2012 Hindawi.

because of their advantages over PVD techniques. Essential chemical reactions and dissociations of reactive gases and volatile precursors occurring in CVD process at different pressures with specific flow

rates provide favorable formation conditions for resultant compounds on the substrates. As one of conventional techniques for synthesizing 1D TMO nanocrystals, the CVD process mainly involves

Figure 5 Schematic diagram for the formation mechanism of Cu_2O nanooctahedra. Reprinted with permission from ref. [20]. Copyright 2013 Elsevier.



traditional vapor–liquid–solid (VLS) growth with assistance of metal catalysts.

The VLS growth mechanism was first proposed by Wagner et al. [25] for the growth of silicon (Si) single crystals in 1964 and then extended to 1D nanostructures. The most apparent feature of the VLS growth is the concretionary eutectic alloy particles on the top of 1D nanostructures, which can be directly identified by TEM observations. Figure 6 shows typical TEM and HRTEM images of TMO NWs formed through VLS mechanism [26–28]. The VLS growth has the advantages that the products can be predicted by phase diagram and the sizes and shapes of formed 1D nanostructures can be controlled by selecting the metal catalysts. Moreover, the fabrication of nanoarrays with certain patterns can be achieved by arranging the metal particles in advance. However, for the materials with very high melting points (such as Fe, 1540 °C), the traditional VLS growth seems not to be applicable. Composite catalysts were developed to resolve this issue. For instance, Tang et al. [29] reported a combined method to synthesize Ga_2O_3 NWs by heating Ga with SiO_2 and Fe_2O_3 . In this

method, the metallic catalyst (Fe) and assistant catalyst (Si) are produced by the reactions between Ga and related oxides. Si can effectively reduce the melting point of catalysts, and the liquid eutectic alloys for initiating the VLS growth can form at the reaction temperature (950 °C) which is much lower than the melting point of Fe. Similar methods have been adopted to synthesize other metal oxide NWs such as MgO [30], SnO_2 [31], and In_2O_3 [32, 33].

Liquid-phase growth

Massive nanoarrays composed of 1D NWs have been fabricated by liquid-phase growth techniques, i.e., template-based synthesis [34]. In the template-based synthetic process, 1D nanostructures are growing in templates within confined space. For instance, hexagonally ordered porous anodic aluminum oxide (AAO) membranes [35] contain cylindrical pores of uniform diameters ranging from ~ 10 to 200 nm. These pores provide the porous channels for the growth of 1D nanostructures. The diameter and length of NWs depend on the pore diameter and the

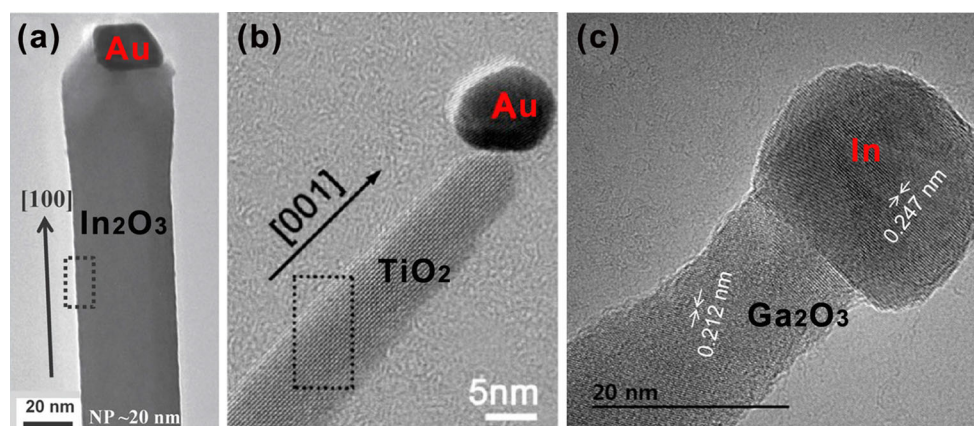


Figure 6 **a** Typical TEM image of VLS growth In_2O_3 nanowire (NW), reprinted with permission from ref. [26]. Copyright 2012 The Royal Society of Chemistry. **b** HRTEM image of TiO_2 NW,

reprinted with permission from ref. [27]. Copyright 2012 American Chemical Society. **c** HRTEM image of Ga_2O_3 NW. Reprinted with permission from ref. [28]. Copyright 2016 Elsevier.

thickness of applied AAO templates. The preparation methods based on template synthesis mainly involve electrochemical deposition [36] and sol-gel deposition [37]. Xu et al. [38] synthesized highly ordered 3D Ni-TiO₂ core-shell nanopillar arrays consisting of anatase TiO₂ outer layer and Ni nanopillar current-collecting arrays by combining the nanoimprinted AAO template technique and atomic layer deposition. Figure 7 shows typical SEM images of AAO template, Ni nanopillar arrays, and 3D Ni-TiO₂ core-shell nanoarrays. Firstly, a thick layer of Ni was electrochemically deposited on top of the AAO template as current-carrying substrate. Subsequently, 3D Ni nanopillar arrays were electrochemically deposited in Watt's bath as electrolyte. The 3D Ni-TiO₂ core-shell nanoarrays were fabricated by depositing a 40-nm-thick layer of TiO₂ on the surface of as-prepared Ni nanopillar arrays. Finally, the AAO template was removed in a 5 wt% H₃PO₄ solution at 30 °C. The sol-gel method, which involves the evolution of integrated inorganic networks through colloidal solutions and gelatinized colloidal solutions in liquid phases, is widely used to synthesize 1D TMO nanostructures [39]. The gelatinized colloidal solutions are incorporated into the pores of AAO templates. After drying and heating, the anticipated NWs can be obtained in AAO templates. Recently, sol-gel template methods are used to prepare various multipartite [40] and composite [41] 1D TMO nanostructures. For instance, cobalt ferrite (CoFe₂O₄) NWs have been successfully synthesized by a sol-gel route

using AAO template [40]. Pirouzfard et al. [42] optimized the parameters of calcination temperature and pH value to prevent the autocombustion of the gel which could cause cracks in the NWs.

Apart from the above methods, thermal oxidation is another facile technique to fabricate 1D TMO nanostructures. Yuan et al. have synthesized CuO [43], ZnO [44], and Fe₂O₃ [45] NWs by thermal oxidation method and proposed a stress-driven growth mechanism for these NWs. In the stress-driven mechanism, the formation of TMO NW is stimulated by compressive stress generated by the volume change accompanying the interfacial reaction during layered oxide growth. Cai et al. [46] reported the detailed microstructural investigation of Fe₂O₃ NWs using HRTEM. They observed three different morphologies, namely single-crystalline, bicrystalline, and tricrystalline NWs. Bicrystalline and tricrystalline wires were demonstrated to result from coalescence of single NWs during the growth process. Specially, a modulated structure is observed in the single-crystalline Fe₂O₃ NWs, as shown in Fig. 8. Based on the HRTEM observations, they proposed a formation process of the modulated structures in single-crystalline NWs, as shown in Fig. 9. During the growth process, shear stress is produced inside the Fe₂O₃ NWs because of the compressive stress as mentioned above. As the shear stress becomes larger and larger, stacking faults will form and the periodical appearance of stacking faults leads to the modulated structures in the single-crystalline Fe₂O₃ NWs.

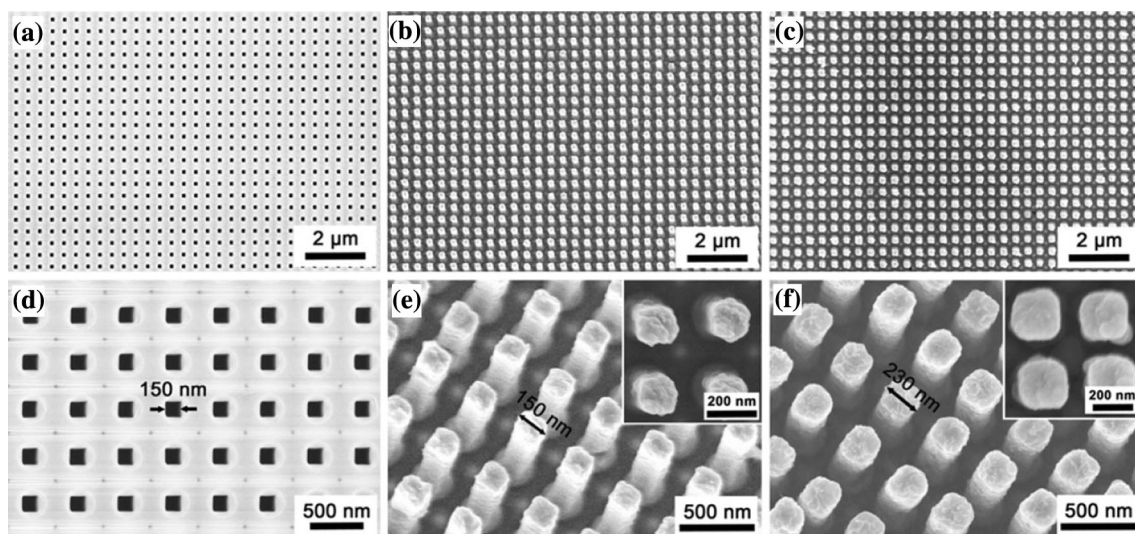


Figure 7 SEM images of the AAO template (a, d), Ni nanopillar arrays (b, e), and 3D Ni-TiO₂ core-shell nanoarrays (c, f). Insets in e and f are the corresponding top-view images. Reprinted with permission from ref. [38]. Copyright 2015 American Chemical Society.

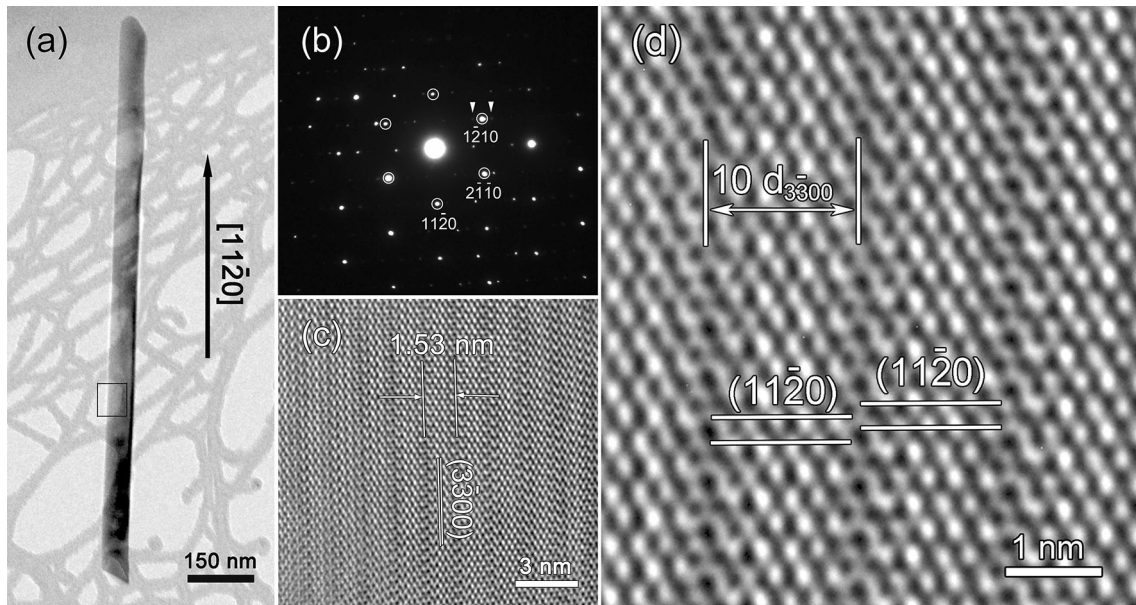
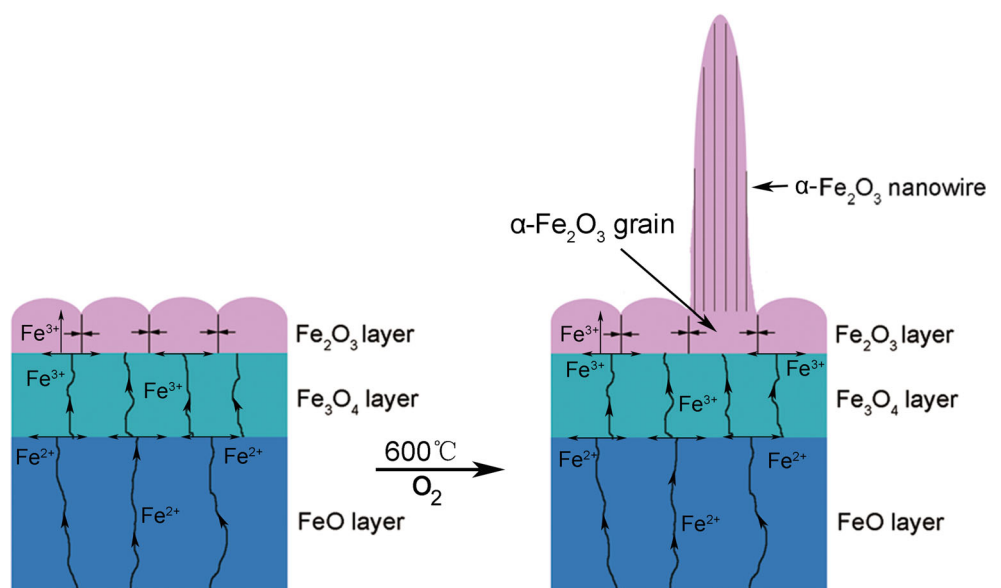


Figure 8 **a** TEM image and **b** SAED pattern of single-crystalline Fe_2O_3 NW. **c** HRTEM image corresponding to the square region marked in **a**. **d** Magnified HRTEM image of **c**. Reprinted with permission from ref. [46]. Copyright 2012 Springer.

Figure 9 Schematic illustration of the formation process for the modulated structure in single-crystalline Fe_2O_3 NW. Reprinted with permission from ref. [46]. Copyright 2012 Springer.



2D nanostructures

Two-dimensional nanostructures with nanoscale thickness and infinite planar dimensions possess unique electronic and optical attributes. Many advanced techniques are developed to fabricate 2D nanostructures. Magnetron sputtering [47–49] is a routine preparation method for high-quality 2D TMO nanostructures such as nanofilms and superlattices.

By the bombardment of energetic ions generated in glow-discharge plasma, the surface atoms or molecules of target are detached from bulk materials and deposited onto substrates to form 2D nanofilms. In the magnetron sputtering system, the ion current delivered to the growing film depends on the strength and design of the magnetic array in the magnetron. This technique allows the ion current to be controlled and optimized at all stages of the

deposition process. Furthermore, pulsed laser deposition is a new technique to prepare multiple TMO films. The target materials are melted under the high-power pulsed laser beam which can produce immense heat and lead to a high temperature. Then the nanofilms are fabricated by deposition of the products of melted raw materials including plasma, ions, atoms, and molecules.

So far, three different growth modes have been reported for the TMO epitaxial films, which include a layer-by-layer growth [50, 51], an island growth [52–55] and a layer by layer plus an island growth [56–60]. The growth mode is greatly influenced by interfacial energy generated during the growth process of epitaxial films. If the growing layer is thinner than a critical thickness, the strain generated by lattice mismatch is elastically accommodated within the growth layer, and a coherent interface will eventually be produced. If the film thickness exceeds the critical thickness, the introduction of misfit dislocations is energetically favored and the strain will be partially relieved to form a semicoherent interface [61, 62].

Cai et al. [63] observed two different growth modes for epitaxial manganite films, as shown in Fig. 10, an island growth mode for $\text{Bi}_{0.4}\text{Ca}_{0.6}\text{MnO}_3$ (BCMO) epitaxial films and a layer-by-layer growth mode for $\text{La}_{0.67}\text{Ca}_{0.33}\text{MnO}_3$ (LCMO) epitaxial films. To explain the formation mechanism of perovskite manganite films, they proposed an atomic collapse model based

on the critical thickness theory. Figure 11 shows the schematic diagrams of the atomic collapse model. When the film is thinner than the critical thickness, the strain caused by the lattice mismatch can be accommodated by elastic deformation. The interface between the epitaxial film and the substrate is coherent without dislocations. When the film grows up to the critical thickness, the strain can no longer be accommodated by elastic deformation. And then misfit dislocations form to relax the strain. Meanwhile, the atoms begin to collapse at the central location of the misfit lattices, leading to the formation of collapse morphology as an island. Maintenance of the collapse morphology depends on the surface atomic diffusion length. That is to say, if the atomic diffusion length is long enough for the surface atoms to diffuse to the lower energy places, the collapse morphology will coalesce and disappear eventually. However, if the atomic diffusion length is short, the collapse morphology will preserve. The proposed atomic collapse model can shed light on the growth modes for other TMO epitaxial films. The observed layer-by-layer growth mode for LCMO on NdGaO_3 [64] and granular-like surface features of LCMO on LaAlO_3 [65] are consistent with the predictions of the atomic collapse model.

Figure 10 TEM and atomic force microscope (AFM) images for BCMO/STO (a, b) and LCMO/STO (c, d) epitaxial films. Reprinted with permission from ref. [63]. Copyright 2013 The American Ceramic Society.

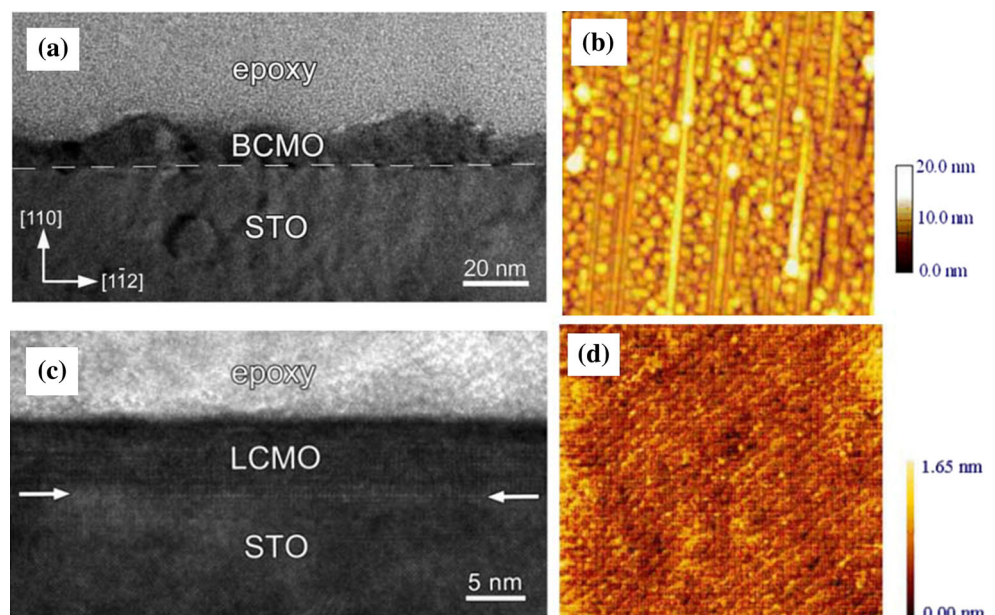
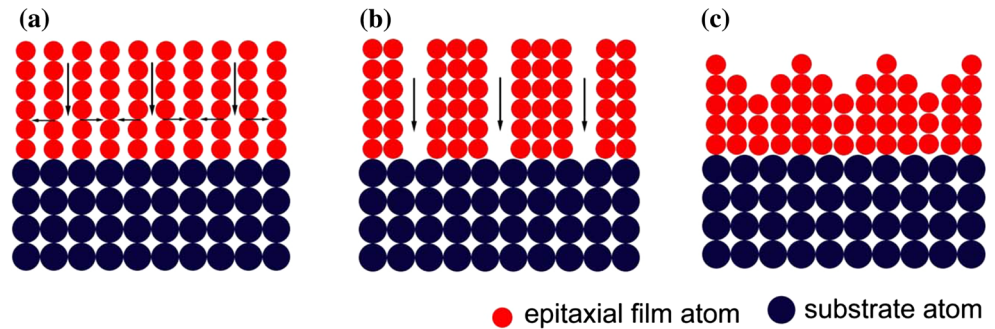


Figure 11 Schematic diagrams for the atomic collapse model. Reprinted with permission from ref. [63]. Copyright 2013 The American Ceramic Society.



Applications of various TMO nanostructures in electronic and photonic devices

Various TMO nanostructures have a wide range of applications in nanoelectronic and photonic devices because of their unique structural properties. For example, 1D morphology is suitable for the fabrication of building blocks because the unrestricted length scale allows them to contact the macroscopic world for many physical measurements [66]. Two-dimensional nanostructures with atomic or molecular thickness and infinite planar dimensions possess extraordinary electronic properties [67]. Zero-dimensional nanoparticles have the advantages of exposing particular surfaces with high activity and large specific surface area. In this section, we present the latest achievements of TMO nanostructure-based electronic and photonic devices.

Photodetectors

Photodetector, which converts light into electricity, has been widely used as binary switching in nanodevices such as field-effect transistors [68], single-electron transistors [69], and intermolecular crossed junctions [70]. TMO nanostructures have been demonstrated with exciting possibilities for use in optoelectronic circuits, especially for 1D nanostructures with excellent sensitivity, superior quantum efficiency, and fast response speed. A comprehensive review on 1D nanostructure photodetectors was published in 2009, in which the performances of single-phase TMO-based detectors were well summarized [71]. Thus, in this section, we focus on the most recent development of binary and ternary oxides such as ZnS–ZnO [72], CuO–TiO₂ [73], and In₂Ge₂O₇ [74]. Fang et al. [72] successfully synthesized side-to-side single-crystalline ZnS–ZnO biaxial

nanobelts by using a facile thermal evaporation process. Figure 12 shows an individual ZnS–ZnO nanobelt-based photodetector built via a lithography-based process, as well as its photoelectric properties used as ultraviolet (UV) light sensors. It can be seen that the as-fabricated UV light sensor possesses a high responsivity to light with a wavelength below 400 nm and a fast response speed. The enhanced performance of ZnS–ZnO biaxial nanobelt was ascribed to suitable band energy alignment of ZnS and ZnO, where a type-II heterojunction was produced at the interface of ZnS and ZnO phases. The existence of such heterojunction facilitates the formation of a charge transfer state and the spatial separation of the photo-excited carriers within the individual structure.

Ternary oxides are reported to exhibit better properties than binary oxides for applications in electronics and gas sensors. For the ternary oxides, the ratio of components can be adjusted to tune their physical and chemical properties, which may provide more potential applications [75]. Li et al. [74] synthesized single-crystalline In₂Ge₂O₇ nanobelts using a vapor transport process. The outstanding performance of the as-assembled photodetector has been demonstrated in terms of high sensitivity and selectivity toward deep UV light. As shown in Fig. 13, the device exhibits high responsivity to deep UV light and possesses a large photocurrent under illumination by 230 nm light as well as reproducible photoresponse characteristics.

Energy-harvesting devices

Solar cells

The recent developments of advanced photovoltaic devices mainly focus on two innovative approaches, photoelectrochemical solar cells, and dye-sensitized

Figure 12 **a** SEM image of the sensor composed of a single ZnS–ZnO biaxial nanobelt. **b** I–V curves under dark condition and UV light illumination. **c** Spectral photoresponse measured from the UV light device. **d** The reproducible on/off switching of the device upon 320 nm light illumination. Reprinted with permission from ref. [72]. Copyright 2012 Wiley-VCH.

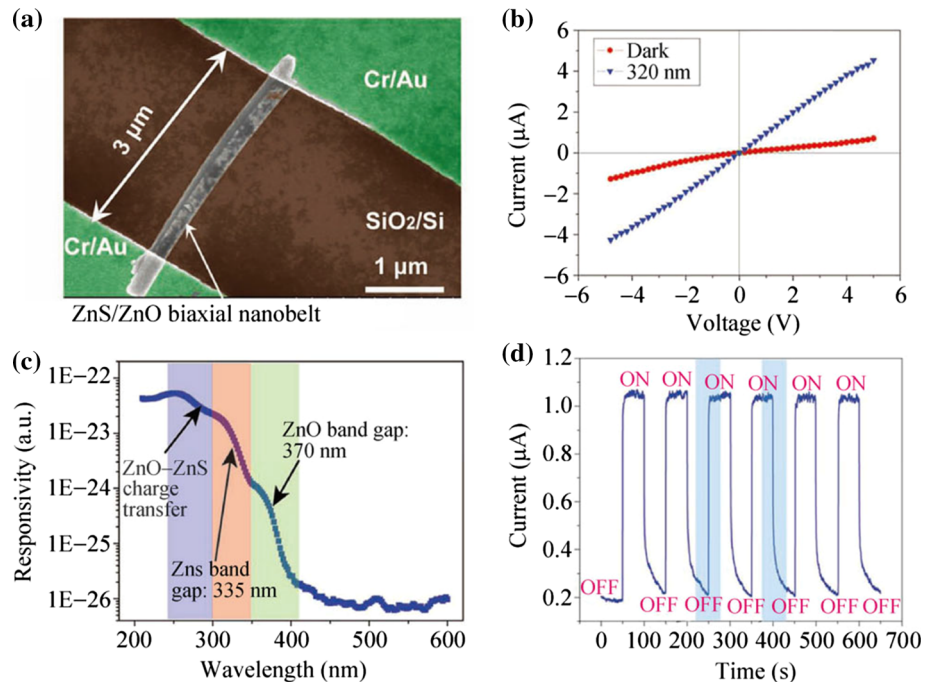
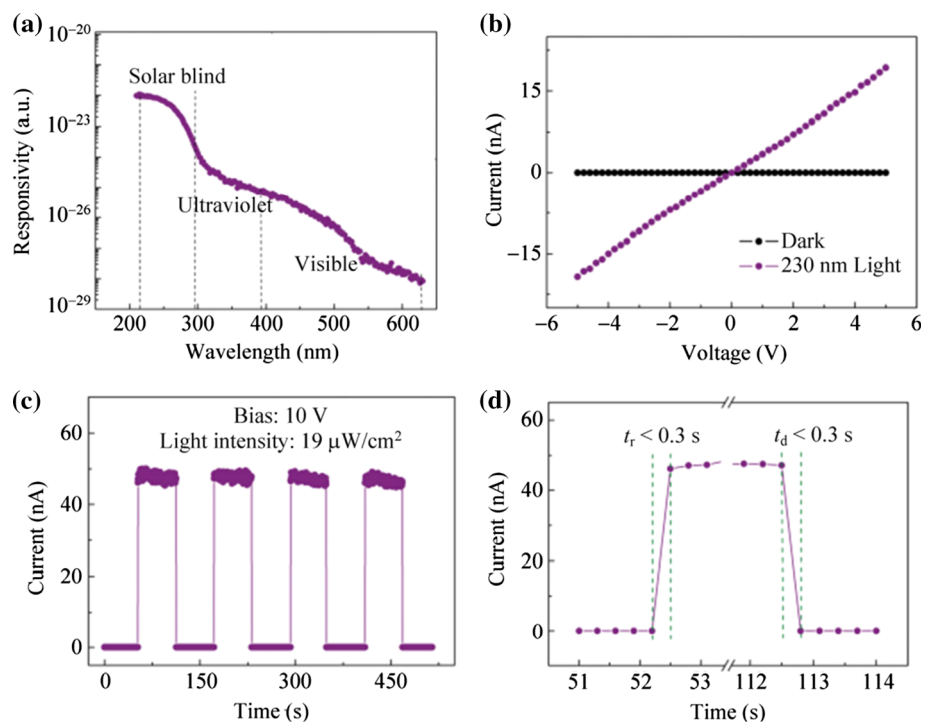


Figure 13 **a** Spectral response of a single In₂Ge₂O₇ nanobelt photodetector. **b** I–V characteristics of the device under 230 nm light irradiation and in the dark. **c** Time response of the photodetector. **d** An enlarged plot of the time response. Reprinted with permission from ref. [74]. Copyright 2010 Wiley-VCH.



solar cells. Dye-sensitized solar cells developed by Grätzel [7] have attracted considerable attention since 1991, which are the most interesting alternatives to conventional solid-state semiconductor solar cells. A typical dye-sensitized solar cell is composed of a mesoporous TiO₂ nanostructured thin film on a transparent conducting oxide (TCO) substrate, whose

surface is covered with a monolayer of dye molecules, a redox-couple electrolyte and a platinumized fluorine-doped tin oxide glass as a counter electrode. The anode reaction is simply the reverse of the cathode reaction and the absorbed photons are transformed into electrons. Many transition metal oxides such as TiO₂, SnO₂, ZnO, WO₃, and Fe₂O₃

have been investigated as possible visible-light-absorbing photoanodes [76–81]. TiO₂ nanomaterials are one of the most widely used semiconductors as a support for dye molecules to harvest sunlight in the electrodes of dye-sensitized solar cells.

To date, the common photoelectrochemical architecture is a several-micron-thick film composed of TiO₂ nanoparticles on TCO substrate. However, the electron diffusion coefficient of these nanoparticulate films is several orders of magnitude smaller than the value in single-crystalline bulk TiO₂, presumably due to electron traps at the contacts between nanoparticles [82]. It has been demonstrated that 1D crystalline NW arrays can be used to construct photoelectrodes and improve charge collection efficiency by promoting charge transport and ion diffusion at the semiconductor–electrolyte interface [83]. Grim et al. [84] synthesized TiO₂ NW arrays on TCO-coated glass substrates by a low-temperature nonpolar solvent/hydrophilic substrate interface hydrolysis reaction. They fabricated dye-sensitized solar cells using TiO₂ NW arrays, which achieved an encouraging photoconversion efficiency of 4.35% with an open-circuit voltage of 0.758 V, a short-circuit current density of 10.2 mA cm⁻², and a fill factor of 0.56. They further modified the TiO₂ NW arrays by coating an overlayer of Nb₂O₅, which can reduce recombination and improve the efficiency. The overall photoconversion efficiency increases to 5.02% with an open-circuit voltage of 0.744 V. The corresponding short-circuit current density and fill factor are enhanced to 10.84 mA cm⁻² and 0.62, respectively. For many years, TMO materials were successfully applied as photoanodes, yielding an overall conversion efficiency more than 11% [85]. Recently, the conversion efficiency has set a new record value exceeding 14% by using porphyrin dye molecule together with cobalt-based redox-couple electrolyte [86]. Figure 14 shows the schematic diagram of the operation principle for the dye-sensitized solar cells and the corresponding J–V curve of solar cell under the illumination of simulated sunlight. The maximum photovoltage obtained in the dye-sensitized solar cell is attributed to the energy gap between the quasi-Fermi level of the TiO₂ and the redox potential of the electrolyte. The efficiency of dye-sensitized solar cells can be improved by increasing the photovoltage using an electrolyte with a quite low redox potential. The optimized cobalt (III/II) complex redox electrolytes were used in the fabrication of the cells. The

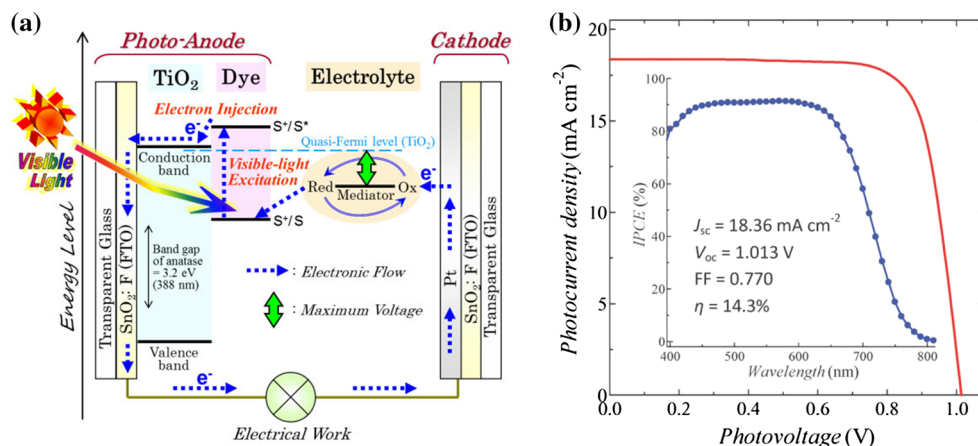
observed high conversion efficiency (over 14%) indicates that this dye-sensitized solar cell has a huge potential to be used as light-to-electric energy conversion devices.

Nanogenerators

As the electronics is developed to be more and more miniaturized and portable, the number of small-sized personality electronic devices, i.e., smart cell phones and watches, is growing drastically. The large-scale distribution makes it impractical to power all portable electronics by batteries considering the inconceivable enormous environmental damage. Therefore, nanogenerators emerge as a new field of nanoenergy to offer a possible solution for the sustainable self-sufficient micro-/nanopower sources by harvesting energy from the environment. Since it was first reported in 2006 [87] that an electric voltage/current was generated as an AFM tip swept across a vertically grown ZnO NW, various ZnO-based nanogenerators have been developed to generate electricity using piezoelectric and pyroelectric effects. The piezoelectric and pyroelectric effects can be used to harvest mechanical energy and thermal energy, respectively. For piezoelectric nanogenerator, the working mechanism is the coupling between the piezoelectric and semiconducting properties of ZnO NWs. The fundamental principle of electricity generation is that a piezoelectric potential forms when the central symmetry in the crystal structure is broken under an external force. Interestingly, the obtained pyroelectric response is associated with the piezoelectric properties of ZnO. In pyroelectric nanogenerator, the charges are produced by the strain-induced anisotropic thermal expansion, which is described as a secondary pyroelectric effect. The thermal deformation can induce a piezoelectric potential difference across the material, which can drive the electrons to flow in the external circuit.

One-dimensional ZnO nanostructures are attracting substantial attention because the NWs can be triggered by tiny physical motions to obtain obvious excitation frequency with a few Hz to multiple MHz, which is ideal for harvesting random energy in the environment. Up to now, ZnO structures in piezoelectric nanogenerators have evolved from a single NW and NW array and then to nanofiber. The power output has been directed along a rapidly ascending path from 9 mV to 37 V [88]. Recently, Hu et al. [89]

Figure 14 **a** Schematic diagram of the operation principle for dye-sensitized solar cell. **b** Typical J–V curve of solar cell under the illumination of simulated sunlight. Inset shows the incident photon-to-electron conversion efficiency spectrum of the cell. Reprinted with permission from ref. [86]. Copyright 2015 The Royal Society of Chemistry.



reported an alternating-current piezoelectric nanogenerator based on vertical ZnO NW arrays. The most striking spot is that a thin layer of poly(methyl methacrylate) (PMMA) was coated on top of the ZnO nanoarrays to serve as an insulating layer and then coated with a metal electrode, as shown in Fig. 15. The thin layer of PMMA between the NWs and the metal electrodes is a key design that contributes to the superior performance. The insulating PMMA layer provides an infinitely high potential barrier, preventing electrons from transporting through the ZnO/metal interface. Furthermore, the PMMA infiltrates into the gap between the ZnO NWs, which helps to transmit the applied stress to all ZnO NWs through the PMMA layer. Therefore, the efficiency of the nanogenerator is greatly enhanced. In addition, it serves as a buffer layer to protect NWs from intimate mechanical interaction with the electrode, thus improving the robustness/durability.

Considering that mechanical and thermal energies are widely available in people's living environment, Wang's group firstly proposed a hybrid cell design which can harvest multiple types of energy

simultaneously to fully utilize the surrounding energy [90]. They integrated a dye-sensitized solar cell and a piezoelectric nanogenerator on the two sides of a common substrate and demonstrated the first hybrid cell for concurrently harvesting solar and mechanical energy. After that, Yang et al. [91] demonstrated a flexible hybrid cell in Fig. 16a, b consisting of a pyroelectric nanogenerator, a piezoelectric nanogenerator, and a solar cell to simultaneously scavenge solar, mechanical and thermal energy. Moreover, the hybrid energy can also be stored in a lithium-ion battery, which can be described as a self-charging power cell [92]. This technology greatly improves the flexibility of energy consumption, so that we can utilize energy to drive electronic devices/systems at any power rate and at any place. The self-charging power cell in Fig. 16c, d is realized by replacing the polyethylene separator used in conventional lithium-ion batteries with a piezoelectric poly(vinylidene fluoride) film, which integrates the characteristics of both piezoelectric and the electrochemical properties.

Figure 15 **a** Fabrication of the piezoelectric nanogenerator. The lower right parts are photos of a fabricated nanogenerator after packaging. **b** Cross-section SEM image of the as-grown ZnO nanoarrays on the substrate. Reprinted with permission from ref. [89]. Copyright 2011 American Chemical Society.

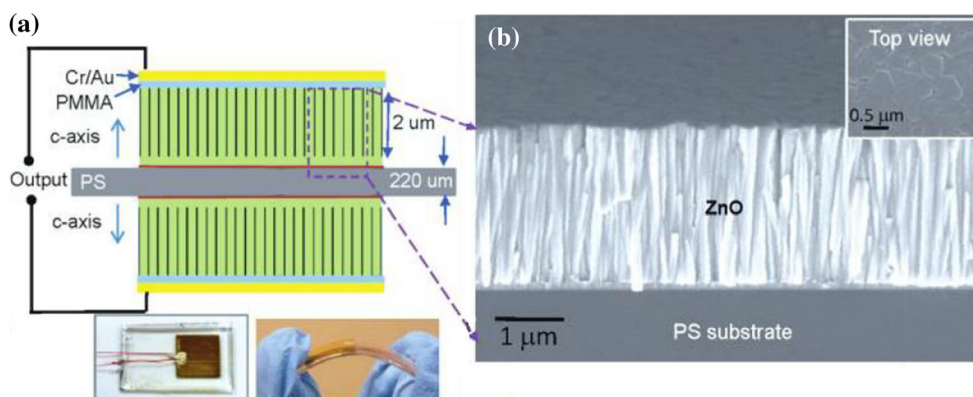
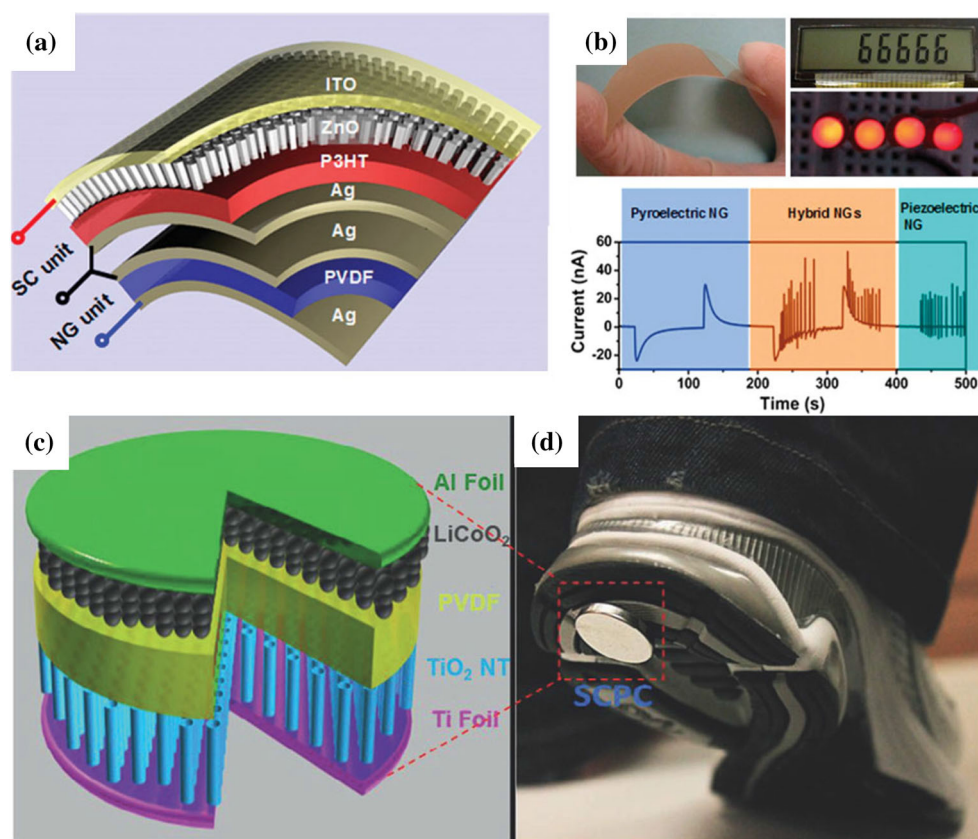


Figure 16 a, b Flexible hybrid energy cell is implemented for simultaneously harvesting thermal, mechanical, and solar energy. Reprinted with permission from ref. [91]. Copyright 2013 American Chemical Society. c Schematic diagram of a self-charging power cell (SCPC). d Sticking a power cell on the bottom of a shoe, the compressive energy generated by walking can be converted and stored directly by SCPC. Reprinted with permission from ref. [92]. Copyright 2012 American Chemical Society.



Energy-storage devices

Energy storage is another equally important technology for energy science besides energy harvesting to generate electricity. The increasing need for cost-effective and environmentally friendly energy for the world's growing population has inspired intensive research for efficient energy-storage systems. Most studies have focused on lithium-ion batteries and supercapacitors. Lithium-ion batteries with high energy density and steady discharge rates have been widely used in daily life such as the powers of computers, mobile phones, watches and toys. Supercapacitor is an attractive energy-storage device due to its high power density (10 kW kg^{-1}), fast charge/discharge rate and long cycle life ($> 10^4$ cycles) [93]. The major requirements of a storage device are high energy, high power density, and fast availability, meaning that the electrode materials should possess high specific capacity and surface area. TMO nanostructures combine the high specific capacity of TMO with high specific area of nanostructures, which are expected to meet the requirements of future energy-storage systems.

Lithium-ion batteries

Rechargeable lithium-ion batteries are based on electrode reactions using classical intercalation reactions for which Li^+ ions are inserted (or extracted) from an open host structure with a concomitant addition (or removal) of electrons. Compared with conventional carbon-based anode materials (e.g., graphite), TMO exhibits larger theoretical capacities, which prompts intensive research for use of TMO as anode electrode [94–98]. For instance, the high theoretical capacity (890 mAh g^{-1}) of Co_3O_4 is more than two times larger than that of graphite (372 mAh g^{-1}). In spite of the high theoretical capacity, TMO nanostructures fall short of satisfying needs for severe mechanical strains and rapid capacity decay because of large volume variation during Li^+ ions insertion/extraction processes [99]. Li et al. [100] fabricated Co_3O_4 nanotubes, nanorods, and nanoparticles and systematically investigated the corresponding electrochemical performances as anode materials. For three Co_3O_4 nanostructures, the discharge capacity decreased dramatically with increasing cycles. After 100 cycles, the capacities

dropped to 55.2 ~ 58.8% of the initial capacity. In addition, a common shortage of TMO materials for electrode is their unfavorable conductivity [101]. A variety of appealing strategies of structural modification have been utilized to solve these intractable problems such as the use of carbon-based nanocomposites. Wu et al. [102] anchored Co_3O_4 nanoparticles on conducting graphene as an anode material for lithium-ion battery. The electrochemical performance of the as-prepared Co_3O_4 /graphene composite is evaluated by galvanostatic charge/discharge cycling at a current density of 50 mA g^{-1} . From Fig. 17, it can be seen that the Co_3O_4 /graphene composite exhibits superior lithium-ion battery performance than graphene or Co_3O_4 . The reversible capacity of the Co_3O_4 /graphene composite is much better than those reported previously, such as unique Co_3O_4 nanostructures and carbon nanofiber/ Co_3O_4 composites [103, 104]. Graphene framework is beneficial for efficiently preventing volume

expansion/contraction and aggregation of Co_3O_4 during the lithium charge/discharge process. The maximum utilization of electrochemically active Co_3O_4 and graphene is achieved by anchoring Co_3O_4 nanoparticles on the graphene sheets.

Afterward, much effort has been devoted to developing new electrode materials to replace toxic and expensive Co-containing materials. CuO has been explored as one of the promising anode materials for lithium-ion batteries due to its high theoretical capacity, high safety, environmental benignity and low cost. The CuO/graphene nanocomposites synthesized by Wang et al. [105] exhibit remarkably enhanced electrochemical and cycling performances compared with pure CuO urchin-like structures, as anode materials in lithium-ion batteries. During the 100 discharge–charge cycles under a current density of 65 mA g^{-1} , the CuO/graphene electrode can stably deliver a reversible capacity of 600 mAh g^{-1} .

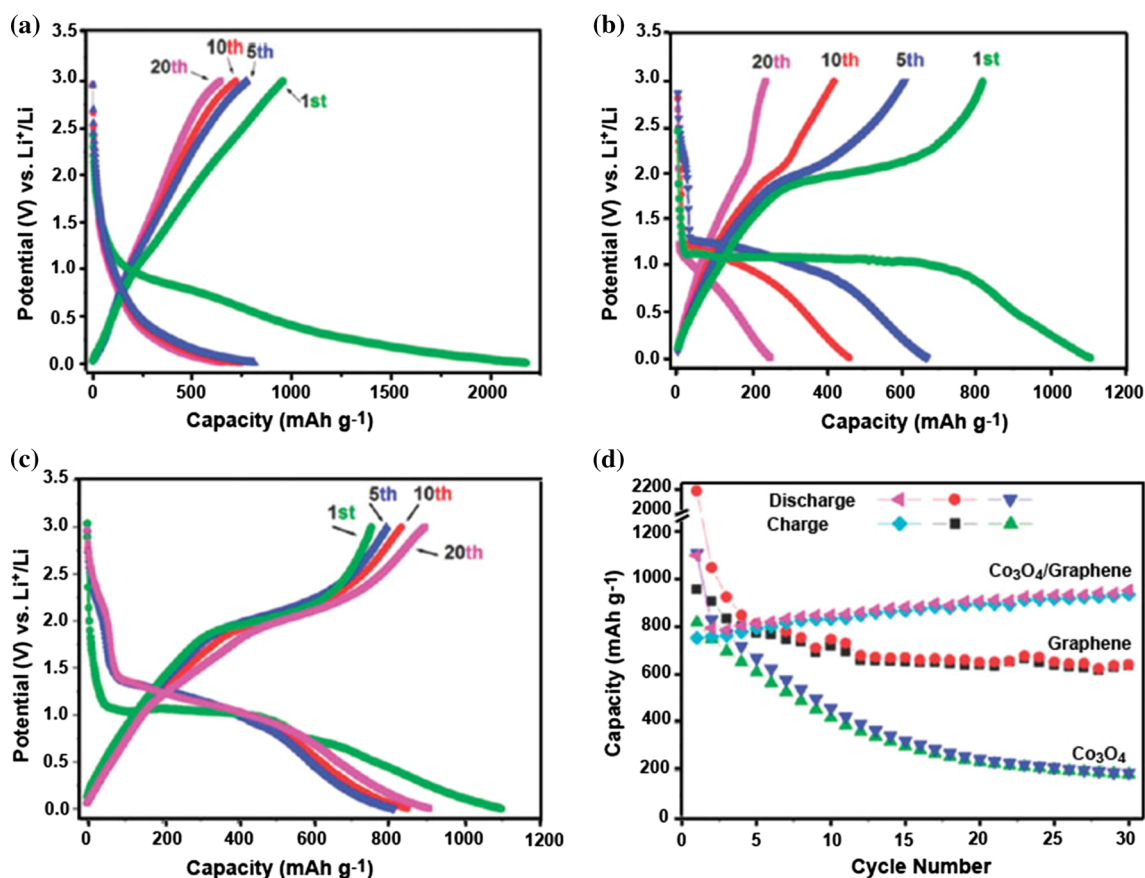


Figure 17 Electrochemical performance of the as-prepared Co_3O_4 /graphene composite. Galvanostatic charge–discharge curves of **a** graphene, **b** Co_3O_4 , and **c** Co_3O_4 /graphene composite. **d** Cycling

performance of graphene, Co_3O_4 and the Co_3O_4 /graphene composite. Reprinted with permission from ref. [102]. Copyright 2010 American Chemical Society.

Recently, hybrid TMO anode materials have been developed to improve the energy density, safety and life cycle of lithium-ion batteries. The combination of different TMO materials can inspire a high capacity which may be close to the theoretical capacity. For instance, $\text{TiO}_2/\alpha\text{-Fe}_2\text{O}_3$ core/shell arrays on carbon textiles fabricated by Luo et al. [106] demonstrate a high discharge capacity of 480 mAh g^{-1} that is equal to 93% of the theoretical capacity (517.3 mAh g^{-1}). In addition, SnO_2 (790 mAh g^{-1}) and Fe_2O_3 (1007 mAh g^{-1}) have been proved to be possible candidates for anode materials because of their high theoretical capacity. $\text{SnO}_2/\text{Fe}_2\text{O}_3$ hybrid nanomaterials with different morphologies are fabricated, exhibiting high reversible capacities. Figure 18a shows a branched nanoheterostructure composed of SnO_2 NW stem and Fe_2O_3 nanorod branches synthesized by Zhou et al. [107]. The branched $\text{Fe}_2\text{O}_3/\text{SnO}_2$ nanoheterostructures show a remarkably improved initial discharge capacity of 1167 mAh g^{-1} and exhibit a poor cycling performance with an initial irreversible loss of 30.6%, as shown in Fig. 18b. Moreover, Zeng et al. [108] fabricated a $\text{Fe}_2\text{O}_3/\text{SnO}_2$ composite nanotube array (shown in Fig. 19) for the anode material, which presents high and stable capacity per unit weight ($\sim 965 \text{ mAh g}^{-1}$) after 50 cycles under a current density of 0.1 mA cm^{-2} ($\sim 132.7 \text{ mA g}^{-1}$). In general, the electrochemical properties of hybrid TMO are much better than monophase TMO materials, as shown in Table 1.

Supercapacitors

The outstanding energy-storage properties of supercapacitors make them suitable for applications in the fields of future consumer electronics and hybrid electric vehicles. According to the charge storage mechanism, supercapacitors can be classified into two kinds: electrical double-layer capacitors and Faradic pseudocapacitors. Carbon-based electrode materials in electrochemical double-layer capacitors, such as graphene, activated carbon and carbon aerogel, store charges by a physical adsorption process at the electrode/electrolyte interface [109]. TMO and conducting polymers are usually used in pseudocapacitors to build up charge storage by fast and reversible surfaces or near-surface reactions [110]. Compared with carbon-based materials, TMO in pseudocapacitors provides higher specific capacitance but have rather poor conductivity. Among the transition metal oxides, MnO_2 is a very promising material for usage in supercapacitors because of its high theoretical specific capacitance (1233 F g^{-1}) and environmentally friendly characteristics [111]. As significant implications of specific surface area for charge storage ability [112], extensive endeavors are aimed at increasing the surface area of TMO electrode materials. To improve the pseudocapacitive properties of MnO_2 , ultrafine MnO_2 NW networks with a specific surface area of $120 \text{ m}^2 \text{ g}^{-1}$ are synthesized by a simple process of hydrothermal treatment [113]. The unique materials exhibit an enhanced specific capacitance (279 F g^{-1}) with high rate capability and good cycling stability than ordinary MnO_2 NWs (167 F g^{-1}) [114]. Likewise, the electrochemical

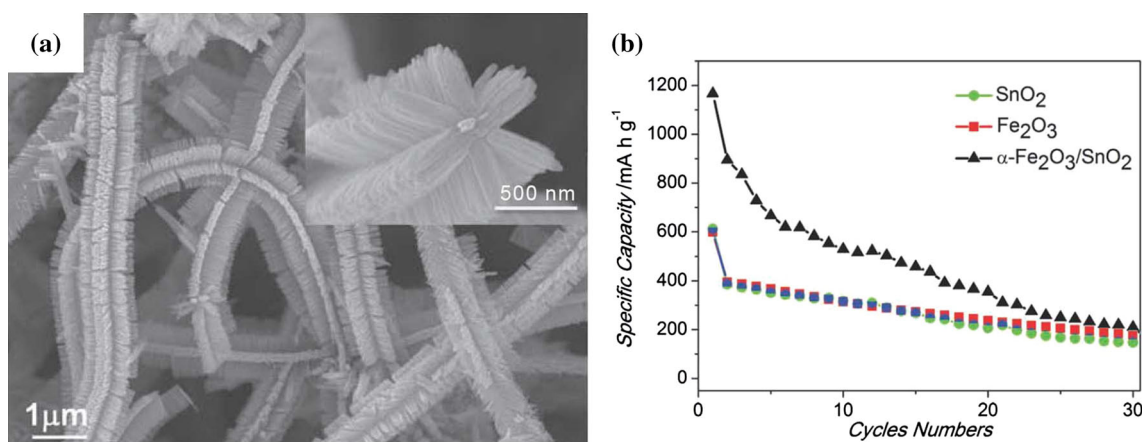


Figure 18 **a** SEM images of $\text{Fe}_2\text{O}_3/\text{SnO}_2$ branched nanostructures. **b** Cycling performance of bare Fe_2O_3 nanorod arrays, SnO_2 NWs, and $\text{Fe}_2\text{O}_3/\text{SnO}_2$ branched nanostructures. Reprinted with permission from ref. [107]. Copyright 2011 Wiley-VCH.

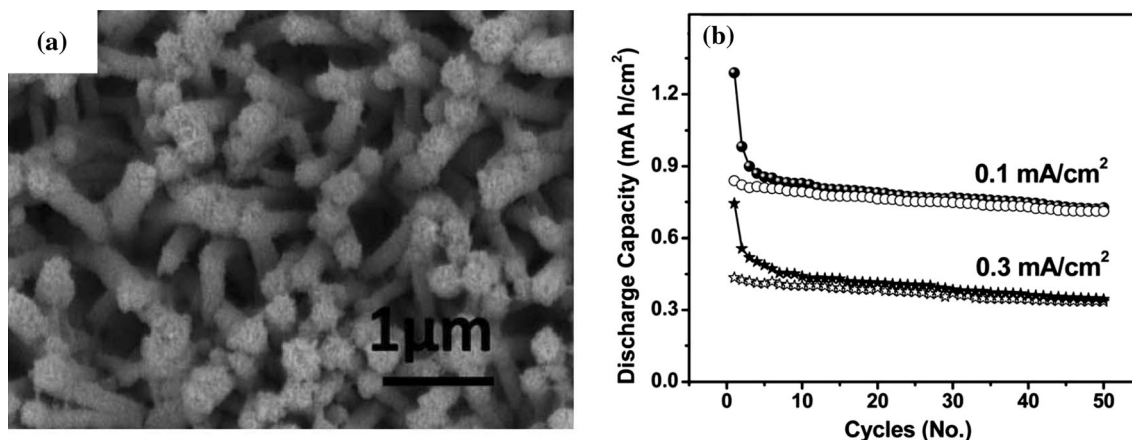


Figure 19 a SEM image and b cycling performance of $\text{Fe}_2\text{O}_3/\text{SnO}_2$ composite nanotube array. Reprinted with permission from ref. [108]. Copyright 2012 The Royal Society of Chemistry.

Table 1 Comparison of electrochemical properties between monophase and hybrid TMO

Monophase and hybrid TMO	Reversible capacity (mAh g^{-1})	Cycle number	Current density (mA g^{-1})
Co_3O_4 nanoparticles [102]	609	5	50
$\text{Co}_3\text{O}_4/\text{graphene}$	935	30	50
CNT- Co_3O_4 [103]	900	50	100
CNF- Co_3O_4 [104]	881	100	50
CuO [105]	400	5	65
CuO/graphene	600	100	65
Fe_2O_3 [108]	700	50	132.7
$\text{SnO}_2/\text{Fe}_2\text{O}_3$ nanotube array	965	50	132.7
$\text{TiO}_2@x\text{-Fe}_2\text{O}_3$ core-shell arrays [106]	480	150	120

performance of nanoscale CuO is highly dependent on their morphology. Dubal et al. [115–117] fabricated a series of CuO nanostructures including nanosheets, microrose-like and microwoolen-like nanosheet clusters, and obtained specific capacitances in the range of $110\text{--}400 \text{ F g}^{-1}$. Porous nanosheet-like CuO films have demonstrated to possess a remarkably higher specific capacitance (566.33 F g^{-1}) than porous nanorod-like CuO films (211.87 F g^{-1}) [118]. It was pointed out that the enhanced porosity of nanosheet-like films was allowed for more electrolyte penetration and the charge storage was hence increased.

In addition to the structural fabrication of electrode materials, another effective strategy for improving pseudocapacitive performance is to enhance electronic conductivity by combining TMO with highly conductive materials. For example, the hybrid structures made of nanoporous Au and nanocrystalline MnO_2 have exhibited a high specific capacitance of

the constituent MnO_2 ($\sim 1145 \text{ F g}^{-1}$), which is close to the theoretical value [119]. Considering the high value of Au, carbon-based substrates have been explored as an attractive candidate because of low cost and enormous progress has been made. Sun et al. [120] fabricated a hierarchical core-shell structure by depositing ultrathin MnO_2 nanoflakes on carbon nanotube networks (CNTs)/Ni mesh. The $\text{MnO}_2@$ -CNTs/Ni nanostructures have given a high specific capacitance of 1072 F g^{-1} in three-electrode configuration. And then a symmetric supercapacitor is assembled using two pieces of $\text{MnO}_2@$ -CNTs/Ni electrodes and Na_2SO_4 solution as electrolyte, as shown in Fig. 20a. The electrochemical measurement results, as shown in Fig. 20b–d, illustrate that the assembled symmetric supercapacitor exhibits wide working voltage (2.0 V), high power density (30.2 kW kg^{-1}), good stability, and long cycle life.

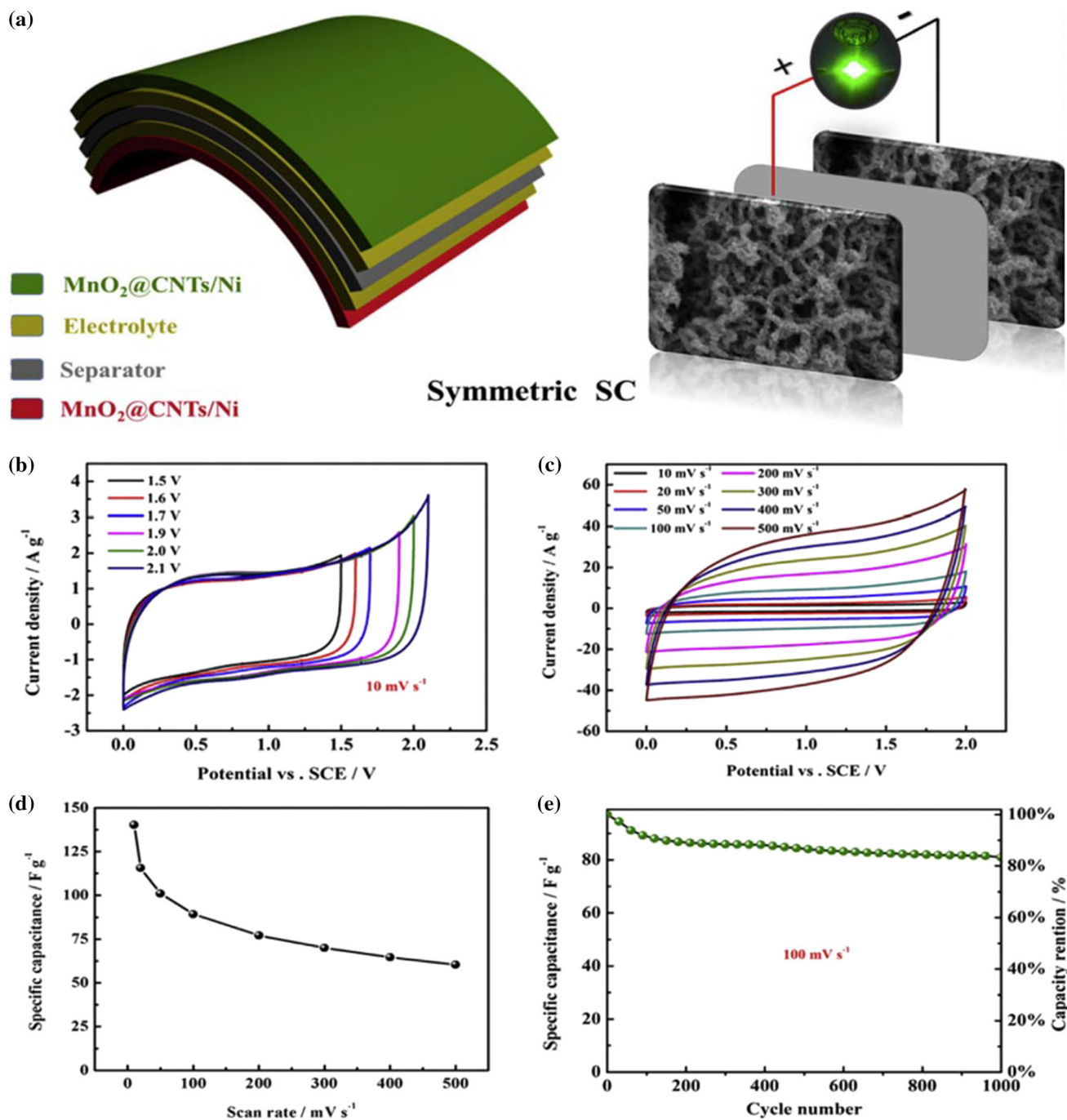


Figure 20 a Schematic structure of the flexible $\text{MnO}_2@\text{CNTs}/\text{Ni}$ -based symmetric supercapacitor. b CV curves at different voltage windows. c CV curves at different scan rates. d Specific

capacitances at different scan rates. e Cycling performance at 100 mV s^{-1} for 1000 cycles. Reprinted with permission from ref. [120]. Copyright 2016 Elsevier.

Photocatalysis

Since, in 1972, Fujishima and Honda [121] firstly developed water splitting to produce hydrogen in a photoelectrochemical process, photocatalysis has attracted strong research interest, and many other

researchers extended it to photo-oxidation or reduction of organic and inorganic substances. In 1976, Carey et al. [122] raised the curtain on the age of environmental applications of semiconductor photocatalysis. Particularly, photodegradation of hazardous chemical wastes is receiving more and more

emphasis. More than a hundred of pollutants have been investigated and can be destructed or transformed by semiconductor photocatalysts at room temperature. In contrast with the conventional approaches such as high-temperature incineration, anaerobic digestion, and conventional physicochemical treatment, semiconductor photocatalysis with low cost and easy operation has tremendous application foreground in water and air purification.

For photocatalysts, their structure and surface properties play an important role in the performance of materials. For TiO_2 , it has three phases, namely anatase, rutile, and brookite. Anatase and rutile TiO_2 are extensively investigated because of their high photocatalytic activity. As shown in Fig. 21, both anatase and rutile phases are composed of bonded TiO_2 octahedron units. However, they have different distortion and arrangement of octahedron units, which contributes to their different density and electronic structures. Compared with anatase TiO_2 , rutile TiO_2 has a higher atomic density and lower bandgap, meaning that it has fewer surface active sites and higher electron–hole recombination. It is expected that rutile TiO_2 has relatively low activity and the experimental results have verified this hypothesis [123]. The influence of structure on performance is also noticeable for other semiconductor materials. Kato et al. [124] found three phases of BaTa_2O_6 , namely orthorhombic phase, hexagonal phase and tetragonal phase with corresponding photocatalytic activities in a descending order. In addition, intense theoretical and experimental studies

demonstrated that the facets with different surface atomic structures exhibit distinct abilities. Liu et al. [125] summarized the tailored facets of TiO_2 crystals. They reported that the photo-excited electrons and holes in TiO_2 nanocrystals are separated on different facets. For anatase TiO_2 , photocatalytic reduction reactions mainly occur on the {101} facets, while oxidation reactions take place on the {110} facets. Similarly, for rutile TiO_2 , the {110} facets provide active sites for photocatalytic reduction reactions, and the {111}/{101} facets supply locations for photocatalytic oxidation reactions.

However, poor electrochemical performance of TMO is one of the most serious limitations hindering its applications in photocatalysis. Heterogeneity is an efficient strategy for TMO semiconductors to improve photocatalytic activities by suppressing electrons and holes recombination and expanding light absorption dimension. On the one hand, the combination of wide-bandgap and narrow-bandgap materials can help to broaden the light response range. For instance, TiO_2 with a wide bandgap can only be excited by UV light irradiation, whereas the CdS-TiO_2 heterogeneous nanomaterial [126] is responsive to the visible spectrum of the sunlight owing to the narrow bandgap of CdS (2.5 eV). On the other hand, the rational arrangement of band structure by designing the composition of heterogeneous materials is also an effective strategy for improvement. Recently, our group synthesized Cu_2O nanoparticles/ CuO NWs hybrid structures (as shown in Fig. 22a) by thermal reduction of CuO NWs [127]. Compared with pure CuO , the polyhedral $\text{Cu}_2\text{O/CuO}$ hybrid nanostructures exhibit enhanced ability to photodegrade methyl orange under visible light, as shown in Fig. 22b, c. The density functional theory calculations [128] suggest that the enhanced photocatalytic performance is attributed to distinct arrangement of Cu_2O and CuO band structures for electron transition in the heterogeneous photocatalytic system. Both conduction band minimum and valence band maximum of Cu_2O are higher than those of CuO . This distinct position characteristic of band structures for CuO and Cu_2O assures that the photogenerated electrons transfer from Cu_2O to CuO while the holes transfer from CuO to Cu_2O when the $\text{Cu}_2\text{O/CuO}$ system is irradiated by the visible light. Hence, photogenerated electrons and holes can be efficiently separated and perform their own functions

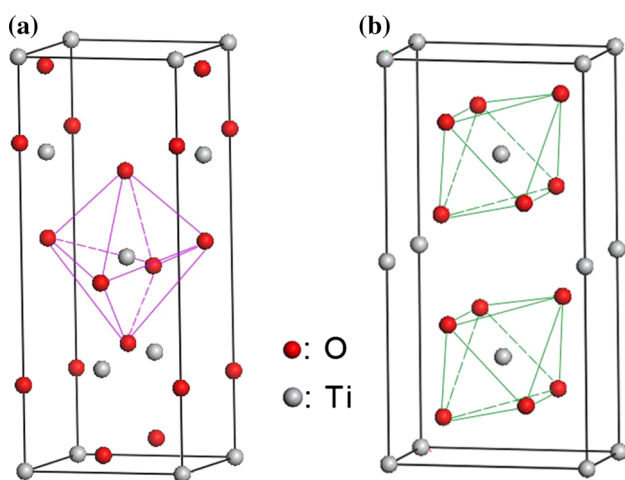
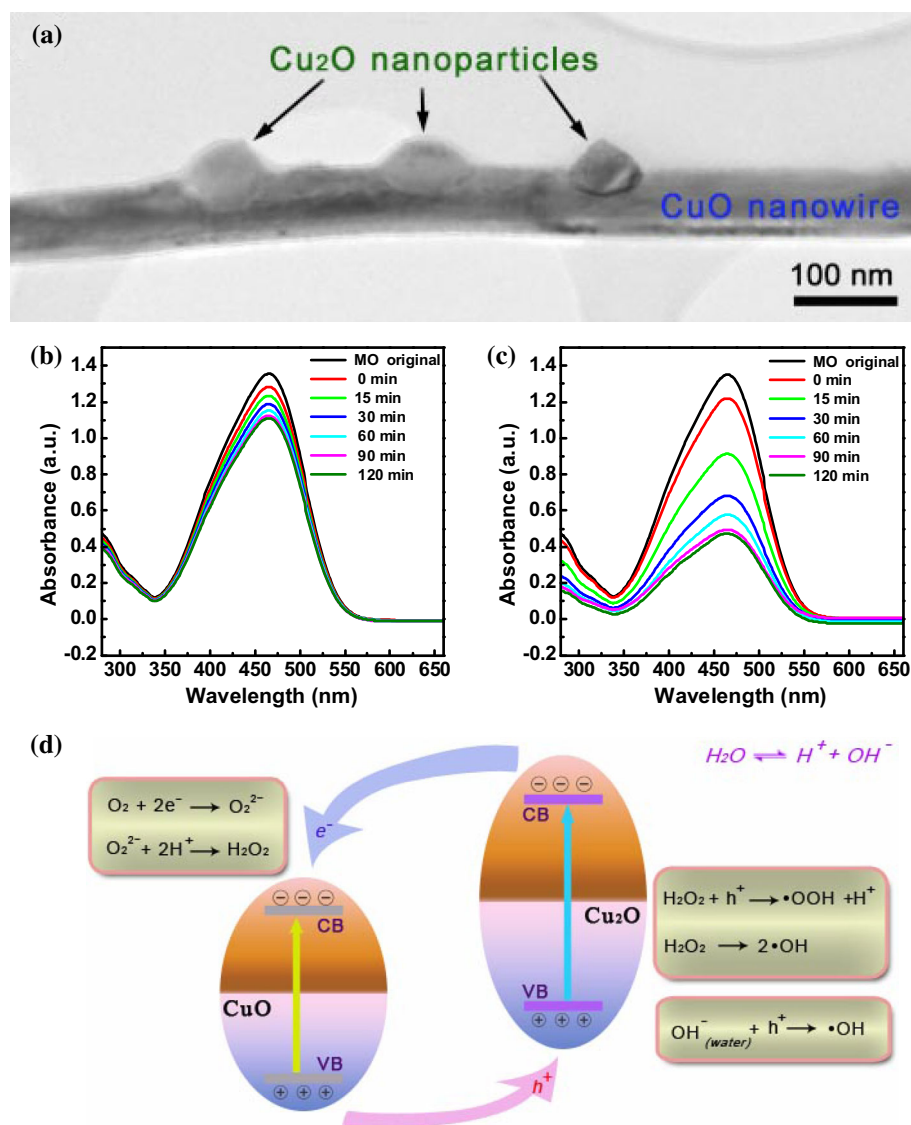


Figure 21 Atomic structure models of **a** anatase and **b** rutile TiO_2 .

Figure 22 a TEM image of $\text{Cu}_2\text{O}/\text{CuO}$ hybrid nanostructure. Photocatalytic activities of b CuO NWs and c $\text{Cu}_2\text{O}/\text{CuO}$ hybrid nanostructures. Reprinted with permission from ref. [127]. Copyright 2014 The Royal Society of Chemistry. d Schematic photocatalytic mechanism in $\text{Cu}_2\text{O}/\text{CuO}$ hybrid system. Reprinted with permission from ref. [128]. Copyright 2016 The Royal Society of Chemistry.



on CuO and Cu_2O to produce the photoreactive oxidant radicals, as shown in Fig. 22d.

The relationship between property and essence of material has always been a remarkable scientific focus for the objective of designing optimal materials for their applications. Much effort has been devoted to enhancing the performances of devices by preparing various TMO nanomaterials and fabricating numerous structures. Investigations on TMO nanomaterials are mainly carried out in two directions including the constituents and structures. The hybridization in constituent and structure of TMO nanomaterials has been demonstrated to be an effective measure for performance improvement, which dominates the developing tendency, as shown in Fig. 23. Multicomponent TMO nanomaterials

afford the intricate electronic system. The combination of TMO and other semiconductors or organic materials achieves tunable bandgap by realignment of energy band. Moreover, the heterostructures, such as core-shell, layer by layer, embedded structures, and metal-organic frameworks (MOFs) [129–131], provide the constraint conditions of electronic motion.

Conclusions and outlook

The recent developments of TMO nanostructures have been highlighted in the aspects of synthesis, characterization, and prominent applications in the fields of photoelectric devices, energy harvest and

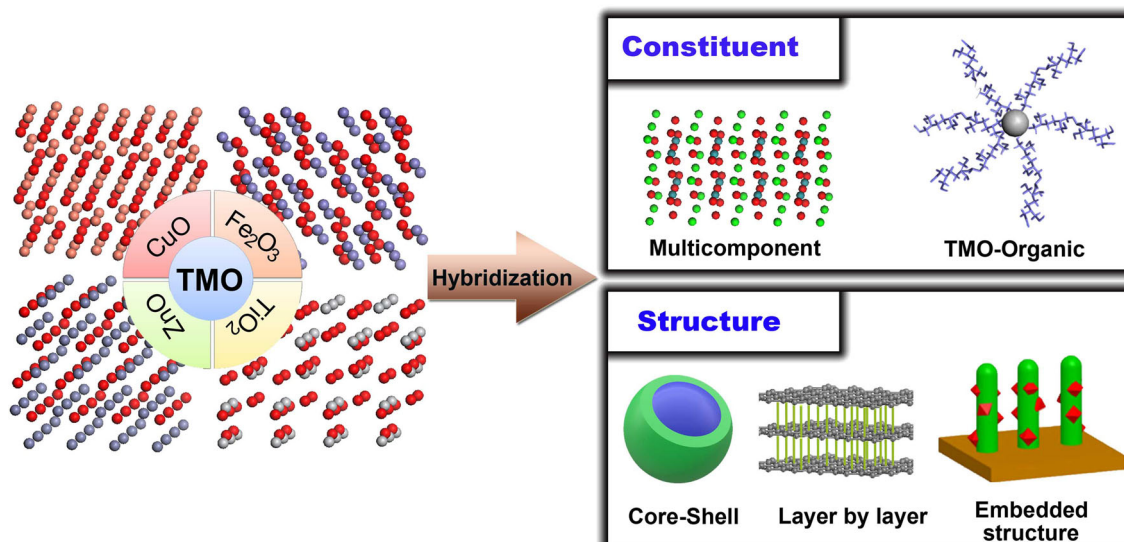


Figure 23 Schematic illustration of the developing trends for TMO nanomaterials.

storage, and environment protection. The mainstream preparation methods of TMO nanostructures with different dimensions and the corresponding growth mechanism are reviewed, which can guide the strategies to fabricate premeditated nanostructures. The internal coordination of microstructure and performance reflected by the corresponding working principles provides guidance for the future development of TMO nanomaterials. Although the extensive investigations of TMO nanostructures have been carried out, significant performance improvements are still required to satisfy the versatile demands in their practical applications. In the future, multi-functional nanodevices will become a research focus for next-generation optoelectronic nanodevices and create a huge commercial potential. As one of the key solution strategies, the utilization of hybrid nanostructures as building blocks for nanodevices will become a hot research field, since the complexity of the components in hybrid nanostructures often gives rise to unique optical and electronic properties. An essential trend in prospective electronics is a gradual shift from all-inorganic and Si-centered devices toward hybrid organic–inorganic devices such as MOFs. The crystalline nanoporous structures of MOFs provide favorable conditions for the assembly of complementary TMO semiconductors and thus MOFs can be implemented as an integral part of solid-state devices. Furthermore, the biggest obstacle to realize practical application of TMO nanostructures is their high cost because of the

sophisticated fabrication techniques. Much more attention should be paid to how to achieve economic industrialization of TMO-based electronic and photonic devices.

Acknowledgements

The authors would like to thank the financial support from the National Key Basic Research Development Program of China (Grant No.: 2012CB722705), the Natural Science Foundation for Outstanding Young Scientists in Shandong Province (Grant No.: JQ201002), and High-end Foreign Experts Recruitment Program (Grant Nos.: GDW20163500110, GDW20173500154). Y. Q. Wang would also like to thank the financial support from the Top-notch Innovative Talent Program of Qingdao City (Grant No.: 13-CX-8), the Taishan Scholar Program of Shandong Province, China, Qingdao International Center for Semiconductor Photoelectric Nanomaterials, and Shandong Provincial University Key Laboratory of Optoelectrical Material Physics and Devices.

References

- [1] Hoffmann MR, Martin ST, Choi WY, Bahnemann DW (1995) Environmental application of semiconductor photocatalysis. *Chem Rev* 95:69–96

- [2] Wu B, Heidelberg A, Boland JJ (2005) Mechanical properties of ultrahigh-strength gold nanowires. *Nat Mater* 4:525–529
- [3] Duan X, Huang Y, Cui Y, Wang J, Lieber CM (2001) Indium phosphide nanowires as building blocks for nanoscale electronic and optoelectronic devices. *Nature* 409:66–69
- [4] Afkhami A, Hashemi P, Bagheri H, Salimian J, Ahmadi A, Madrakian T (2017) Impedimetric immunosensor for the label-free and direct detection of botulinum neurotoxin serotype A using Au nanoparticles/graphene-chitosan composite. *Biosens Bioelectron* 93:124–131
- [5] Li XM, Tao L, Chen ZF, Fang H, Li XS, Wang XR, Xu JB, Zhu HW (2017) Graphene and related two-dimensional materials: structure-property relationships for electronics and optoelectronics. *Appl Phys Rev* 4:021306/1-31
- [6] Khan AH, Ghosh S, Pradhan B, Dalui A, Shrestha LK, Acharya S, Ariga K (2017) Two-dimensional (2D) nanomaterials towards electrochemical nanoarchitectonics in energy-related applications. *Bull Chem Soc Jpn* 90:627–648
- [7] Oregan B, Grätzel M (1991) A low-cost, high-efficiency solar-cell based on dye-sensitized colloidal TiO₂ films. *Nature* 353:737–740
- [8] Huang MH, Mao S, Feick H, Yan HQ, Wu YY, Kind H, Weber E, Russo R, Yang PD (2001) Room-temperature ultraviolet nanowire nanolasers. *Science* 292:1897–1899
- [9] Rao C, Cheetham A (1996) Giant magnetoresistance in transition metal oxides. *Science* 272:369–370
- [10] Poizot P, Laruelle S, Grugeon S, Dupont L, Tarascon J (2000) Nano-sized transition-metal oxides as negative-electrode materials for lithium-ion batteries. *Nature* 407:496–499
- [11] Xie X, Li Y, Liu ZQ, Haruta M, Shen W (2009) Low-temperature oxidation of CO catalysed by Co₃O₄ nanorods. *Nature* 458:746–749
- [12] Varghese J, Whatmore RW, Holmes JD (2013) Ferroelectric nanoparticles, wires and tubes: synthesis, characterisation and applications. *J Mater Chem C* 1:2618–2638
- [13] Han SC, Hu LF, Liang ZQ, Wageh S, Al-Ghamdi AA, Chen YS, Fang XS (2014) One-step hydrothermal synthesis of 2D hexagonal nanoplates of α -Fe₂O₃/graphene composites with enhanced photocatalytic activity. *Adv Funct Mater* 24:5719–5727
- [14] Li JC, Shi XY, Shen MW (2014) Hydrothermal synthesis and functionalization of iron oxide nanoparticles for MR imaging applications. *Part Part Syst Charact* 31:1223–1237
- [15] Lee M, Balasingam SK, Jeong HY, Hong WG, Lee HBR, Kim BH, Jun Y (2014) One-step hydrothermal synthesis of graphene decorated V₂O₅ nanobelts for enhanced electrochemical energy storage. *Sci Rep* 5:8151/1-9
- [16] Feng HL, Li C, Li T, Diao FY, Xin T, Liu B, Wang YQ (2017) Three-dimensional hierarchical SnO₂ dodecahedral nanocrystals with enhanced humidity sensing properties. *Sens Actuators B Chem* 243:704–714
- [17] Siegfried MJ, Choi KS (2006) Elucidating the effect of additives on the growth and stability of Cu₂O surfaces via shape transformation of pre-grown crystals. *J Am Chem Soc* 128:10356–10357
- [18] Siegfried MJ, Choi KS (2008) Elucidation of an overpotential-limited branching phenomenon observed during the electrocrystallization of cuprous oxide. *Angew Chem Int Ed* 47:368–372
- [19] Du QT, Tan JS, Wang QT, Li CY, Liu XH, Cai RS, Ding YH, Wang YQ (2012) Electrochemical deposition and formation mechanism of single-crystalline Cu₂O octahedra on aluminum. *J Anal Methods Chem* 2012:406162/1-8
- [20] Diao FY, Du QT, Li CY, Shang L, Wang YQ (2013) Facile synthesis of cuprous oxide nanooctahedra using electrodeless deposition. *Chem Phys Lett* 587:45–49
- [21] Rackauskas S, Jiang H, Wagner JB, Shandakov SD, Hansen TW, Kauppinen EI, Nasibulin AG (2014) In situ study of noncatalytic metal oxide nanowire growth. *Nano Lett* 14:5810–5813
- [22] Close T, Tulsyan G, Diaz CA, Weinstein SJ, Richter C (2015) Reversible oxygen scavenging at room temperature using electrochemically reduced titanium oxide nanotubes. *Nat Nanotechnol* 10:418–422
- [23] Huang S, Guo CF, Zhang X, Pan W, Luo X, Zhao CS, Gong JH, Li XY, Ren ZF, Wu H (2015) Buckled tin oxide nanobelt webs as highly stretchable and transparent photosensors. *Small* 11:5712–5719
- [24] Lee JH, Katoch A, Choi SW, Kim JH, Kim HW, Kim SS (2015) Extraordinary improvement of gas-sensing performances in SnO₂ nanofibers due to creation of local p–n heterojunctions by loading reduced graphene oxide nanosheets. *ACS Appl Mater Interfaces* 7:3101–3109
- [25] Wagner RS, Ellis WC (1964) Vapor–liquid–solid mechanism of single crystal growth. *Appl Phys Lett* 4:89–90
- [26] Chang WC, Kuo CH, Lee PJ, Chueh YL, Lin SJ (2012) Synthesis of single crystal Sn-doped In₂O₃ nanowires: size-dependent conductive characteristics. *Phys Chem Chem Phys* 14:13041–13045
- [27] Zhuge FW, Yanagida T, Nagashima K, Yoshida H, Kanai M, Xu B, Klamchuen A, Meng G, He Y, Rahong S, Li XM, Suzuki M, Kai S, Takeda S, Kawai T (2012) Fundamental strategy for creating VLS grown TiO₂ single crystalline nanowires. *J Phys Chem C* 116:24367–24372

- [28] Lee SY, Choi KH, Kang HC (2016) Growth mechanism of In-doped β -Ga₂O₃ nanowires deposited by radio frequency powder. *Mater Lett* 176:213–218
- [29] Tang CC, Fan SS, Marclamy D (2001) Silica-assisted catalytic growth of oxide and nitride nanowires. *Chem Phys Lett* 333:12–15
- [30] Marcu A, Grigoriu C, Lungu CP, Yanagida T, Kawai T (2012) Ablation particles parameters influences on VLS oxide nanowire growing. *Physica E* 44:1071–1073
- [31] Nam SH, Boo JH (2012) Rutile structured SnO₂ nanowires synthesized with metal catalyst by thermal evaporation method. *J Nanosci Nanotechnol* 12:1559–1562
- [32] Wang B, Zheng ZQ, Wu HY, Zhu LF (2014) Field emission properties and growth mechanism of In₂O₃ nanostructures. *Nanoscale Res Lett* 9:111/1-8
- [33] Meng G, Yanagida T, Yoshida H, Nagashima K, Kanai M, Zhuge FW, He Y, Klamchuen A, Rahong S, Fang XD, Takeda S, Kawai T (2014) A flux induced crystal phase transition in the vapor–liquid–solid growth of indium-tin oxide nanowires. *Nanoscale* 6:7033–7038
- [34] Hulteen JC, Martin CR (1997) A general template-based method for the preparation of nanomaterials. *J Mater Chem* 7:1075–1081
- [35] Yuan LX, Meng SQ, Zhou YY, Yue ZX (2013) Controlled synthesis of anatase TiO₂ nanotube and nanowire arrays via AAO template-based hydrolysis. *J Mater Chem A* 1:2552–2557
- [36] Kolmakov A, Zhang Y, Cheng G, Moskovits M (2003) Detection of CO and O₂ using tin oxide nanowire sensors. *Adv Mater* 15:997–1000
- [37] Lakshmi BB, Patrissi CJ, Martin CR (1997) Sol–gel template synthesis of semiconductor oxide micro- and nanostructures. *Chem Mater* 9:2544–2550
- [38] Xu Y, Zhou M, Wen LY, Wang CL, Zhao HP, Mi Y, Liang LY, Fu Q, Wu MH, Lei Y (2015) Highly ordered three-dimensional Ni-TiO₂ nanoarrays as sodium ion battery anodes. *Chem Mater* 27:4274–4280
- [39] Huang CM, Chen LH, Xu G, Miao L (2012) Sol–gel template synthesis and characterization of VO₂ nanotube arrays. *J Sol-Gel Sci Technol* 63:103–107
- [40] Chen JY, Wang Y, Deng Y (2013) Highly ordered CoFe₂O₄ nanowires array prepared via a modified sol–gel templated approach and its optical and magnetic properties. *J Alloy Compd* 552:65–69
- [41] Pirouzfard A, Ebrahimi SAS (2014) Optimization of sol–gel synthesis of CoFe₂O₄ nanowires using template assisted vacuum suction method. *J Magn Magn Mater* 370:1–5
- [42] Qu XF, Xie DD, Gao L, Cao LX, Du FL (2015) Synthesis and characterization of TiO₂/WO₃ composite nanotubes for photocatalytic applications. *J Mater Sci* 1:21–27. <https://doi.org/10.1007/s10853-014-8441-7>
- [43] Yuan L, Wang YQ, Mema R, Zhou GW (2011) Driving force and growth mechanism for spontaneous oxide nanowire formation during the thermal oxidation of metals. *Acta Mater* 59:2491–2500
- [44] Yuan L, Wang C, Cai RS, Wang YQ, Zhou GW (2013) Spontaneous ZnO nanowire formation during oxidation of Cu-Zn alloy. *J Appl Phys* 114:023512/1-8
- [45] Yuan L, Wang YQ, Cai RS, Jiang Q, Wang JB, Li BQ, Sharma A, Zhou GW (2012) The origin of hematite nanowire growth during the thermal oxidation of iron. *Mater Sci Eng B* 177:327–336
- [46] Cai RS, Li T, Wang YQ, Wang C, Yuan L, Zhou GW (2012) Formation of modulated structures in single-crystalline hexagonal α -Fe₂O₃ nanowires. *J Nanopart Res* 14:1073/1-11
- [47] Kment S, Hubicka Z, Krysa J, Sekora D, Zlamal M, Olejnicek J, Cada M, Ksirova P, Remes Z, Schmuki P, Schubert E, Zboril R (2015) On the improvement of PEC activity of hematite thin films deposited by high-power pulsed magnetron sputtering method. *Appl Catal B Environ* 165:344–350
- [48] Barnabé A, Thimont Y, Lalanne M, Presmanes L, Tailhades P (2015) P-type conducting transparent characteristics of delafossite Mg-doped CuCrO₂ thin films prepared by RF-sputtering. *J Mater Chem C* 3:6012–6024
- [49] Dixon SC, Scanlon DO, Carmalt CJ, Parkin IP (2016) N-type doped transparent conducting binary oxides: an overview. *J Mater Chem C* 4:6946–6961
- [50] Chang J, Park YS, Lee JW, Kim SK (2008) Layer-by-layer growth and growth-mode transition of SrRuO₃ thin films on atomically flat single-terminated SrTiO₃ (111) surfaces. *J Cryst Growth* 311:3771–3774
- [51] Van HA, Pinxteren HM, Lohmeier M, Vlieg E, Thornton JM (1992) Surfactant-induced layer-by-layer growth of Ag on Ag (111). *Phys Rev Lett* 68:3335–3338
- [52] Wei XH, Zhu J, Li YR (2011) Anisotropic lattice strain relaxation of MgO/SrTiO₃ (001) in a textured island growth mode. *Vacuum* 85:999–1003
- [53] Ait-Mansour K, Dentel D, Kubler L, Diani M, Bischoff JL, Galliano A (2005) Ge epitaxial island growth on a graphitized C-rich 4H-SiC (0001) surface. *J Cryst Growth* 275:e2275–e2280
- [54] Liu D, Liu W (2011) Growth and characterization of epitaxial (La_{2/3}Sr_{1/3}) MnO₃ films by pulsed laser deposition. *Ceram Int* 37:3531–3534
- [55] Ding YH, Cai RS, Du QT, Wang YQ, Chen YZ, Sun JR (2011) Microstructure evolution of Bi_{0.4}Ca_{0.6}MnO₃

- epitaxial films with different thickness. *J Cryst Growth* 317:115–118
- [56] Snyder CW, Barlett D, Orr BG, Bhattacharya PK, Singh J (1991) The molecular beam epitaxy growth of InGaAs on GaAs (100) studied by in situ scanning tunneling microscopy and reflection high-energy electron diffraction. *J Vac Sci Technol B* 9:2189–2193
- [57] LeGoues FK, Copel M, Tromp RM (1990) Microstructure and strain relief of Ge films grown layer by layer on Si (001). *Phys Rev B* 42:11690–11700
- [58] Asai M, Ueba H, Tatsuyama C (1985) Heteroepitaxial growth of Ge films on the Si (100)-2 × 1 surface. *J Appl Phys* 58:2577–2583
- [59] Beck MJ, van de Walle A, Asta M (2004) Surface energetics and structure of the Ge wetting layer on Si(100). *Phys Rev B* 70:205337/1-7
- [60] Liu EZ, Wang CY (2006) Energetics of the growth mode transition in InAs/GaAs (001) small quantum dot formation: a first-principles study. *Surf Sci* 600:2007–2010
- [61] Matthews JW, Mader S, Light TB (1970) Accommodation of misfit across the interface between crystals of semiconducting elements or compounds. *J Appl Phys* 41:3800–3804
- [62] Matthews JW, Blakeslee AE (1974) Defects in epitaxial multilayers: I. Misfit dislocations. *J Cryst Growth* 27:118–125
- [63] Cai RS, Wang YQ, Liu XH, Gao WW, Chen YZ, Sun JR, Wang YG (2013) Origin of different growth modes for manganite epitaxial films. *J Am Ceram Soc* 96:1660–1665
- [64] Jo MH, Mathur ND, Todd NK, Blamire MG (2000) Very large magnetoresistance and coherent switching in half-metallic manganite tunnel junctions. *Phys Rev B* 61:R14905–R14908
- [65] Rao RA, Lavric D, Nath TK, Eom CB, Wu L, Tsui F (1999) Effects of film thickness and lattice mismatch on strain states and magnetic properties of $\text{La}_{0.8}\text{Ca}_{0.2}\text{MnO}_3$ thin films. *J Appl Phys* 85:4794–4796
- [66] Devan RS, Patil RA, Lin JH, Ma YR (2012) One-dimensional metal-oxide nanostructures: recent developments in synthesis, characterization, and applications. *Adv Funct Mater* 22:3326–3370
- [67] Osada M, Sasaki T (2012) Two-dimensional dielectric nanosheets: novel nanoelectronics from nanocrystal building blocks. *Adv Mater* 24:210–228
- [68] Tans SJ, Verschueren RM, Dekker C (1998) Room-temperature transistor based on a single carbon nanotube. *Nature* 393:49–52
- [69] Bockrath M, Cobden DH, McEuen PL, Chopra NG, Zettl A, Thess A, Smalley RE (1997) Single-electron transport in ropes of carbon nanotubes. *Science* 275:1922–1925
- [70] Fuhrer MS, Nygard J, Shih L, Forero M, Yoon Y, Mazzonei MSC, Choi HJ, Ihm J, Louie SG, Zettl A, McEuen PL (2000) Crossed nanotube junctions. *Science* 288:494–497
- [71] Zhai TY, Fang XS, Liao MY, Xu XJ, Zeng HB, Yoshio B, Golberg DA (2009) Comprehensive review of one-dimensional metal-oxide nanostructure photodetectors. *Sensors* 9:6504–6529
- [72] Hu LF, Yan J, Liao MY, Xiang HJ, Gong XG, Zhang LD, Fang XS (2012) An optimized ultraviolet-a light photodetector with wide-range photoresponse based on ZnS/ZnO biaxial nanobelt. *Adv Mater* 24:2305–2309
- [73] Tsai TY, Chang SJ, Hsueh TJ, Hsueh HT, Weng WY, Hsu CL, Da BT (2011) P-Cu₂O-shell/n-TiO₂-nanowire-core heterostructure photodiodes. *Nanoscale Res Lett* 6:575/1-7
- [74] Li L, Lee PS, Yan CY, Zhai YT, Fang XS, Liao MY, Koide Y, Bando Y, Golberg D (2010) Ultrahigh-performance solar-blind photodetectors based on individual single-crystalline In₂Ge₂O₇ nanobelts. *Adv Mater* 22:5145–5149
- [75] Mao YB, Park TJ, Wong SS (2005) Synthesis of classes of ternary metal oxide nanostructures. *Chem Commun* 41:5721–5735
- [76] Park NG (2015) Perovskite solar cells: an emerging photovoltaic technology. *Mater Today* 18:65–72
- [77] Yu Q, Meng XG, Wang T, Li P, Liu LQ, Chang K, Liu GG, Ye JH (2015) A highly durable p-LaFeO₃/n-Fe₂O₃ photocell for effective water splitting under visible light. *Chem Commun* 51:3630–3633
- [78] Gopi CVVM, Venkata-Haritha M, Lee YS, Kim HJ (2016) ZnO nanorods decorated with metal sulfides as stable and efficient counter-electrode materials for high-efficiency quantum dot-sensitized solar cells. *J Mater Chem A* 4:8161–8171
- [79] Qiu M, Zhu DQ, Bao XC, Wang JY, Wang XF, Yang RQ (2016) WO₃ with surface oxygen vacancies as an anode buffer layer for high performance polymer solar cells. *J Mater Chem A* 4:894–900
- [80] Xie KY, Guo M, Huang HT (2015) Photonic crystals for sensitized solar cells: fabrication, properties, and applications. *J Mater Chem C* 3:10665–10686
- [81] Zhang ST, Foldyna M, Roussel H, Consonni V, Pernot E, Schmidt-Mende L, Rapenne L, Jiménez C, Deschanvres JL, Muñoz-Rojas D, Bellet D (2017) Tuning the properties of F:SnO₂ (FTO) nanocomposites with S:TiO₂ nanoparticles-promising hazy transparent electrodes for photovoltaics applications. *J Mater Chem C* 5:91–102
- [82] Fisher AC, Peter LM, Ponomarev EA, Walker AB, Wijayantha KGU (2000) Intensity dependence of the back reaction and transport of electrons in dye-sensitized nanocrystalline TiO₂ solar cells. *J Phys Chem B* 104:949–958

- [83] Law M, Greene LE, Johnson JC, Saykally R, Yang PD (2005) Nanowire dye-sensitized solar cells. *Nat Mater* 4:455–459
- [84] Feng XJ, Shankar K, Varghese OK, Paulose M, Latempa TJ, Grimes CA (2008) Vertically aligned single crystal TiO₂ nanowire arrays grown directly on transparent conducting oxide coated glass: synthesis details and applications. *Nano Lett* 8:3781–3786
- [85] Chen CY, Wang MK, Li JY, Pootrakulchote N, Alibabaei L, Ngoc-le C, Decoppet JD, Tsai JH, Grätzel C, Wu CG, Zakeeruddin SM, Grätzel M (2009) Highly efficient light-harvesting ruthenium sensitizer for thin-film dye-sensitized solar cells. *ACS Nano* 3:3103–3109
- [86] Kakiage K, Aoyama Y, Yano T, Oya K, Fujisawa J, Hanaya M (2015) Highly-efficient dye-sensitized solar cells with collaborative sensitization by silyl-anchor and carboxy-anchor dyes. *Chem Commun* 15:15894–15897
- [87] Wang ZL, Song JH (2006) Piezoelectric nanogenerators based on zinc oxide nanowire arrays. *Science* 312:242–245
- [88] Wang ZL, Zhu G, Yang Y, Wang SH, Pan CF (2012) Progress in nanogenerators for portable electronics. *Mater Today* 15:532–543
- [89] Hu Y, Zhang Y, Xu C, Lin L, Snyder RL, Wang ZL (2011) Self-powered system with wireless data transmission. *Nano Lett* 11:2572–2577
- [90] Xu C, Wang XD, Wang ZL (2009) Nanowire structured hybrid cell for concurrently scavenging solar and mechanical energies. *J Am Chem Soc* 131:5866–5872
- [91] Yang Y, Zhang HL, Zhu G, Lee S, Lin ZH, Wang ZL (2013) Flexible hybrid energy cell for simultaneously harvesting thermal, mechanical, and solar energies. *ACS Nano* 7:785–790
- [92] Xue XY, Wang SH, Guo WX, Zhang Y, Wang ZL (2012) Hybridizing energy conversion and storage in a mechanical-to-electrochemical process for self-charging power cell. *Nano Lett* 12:5048–5054
- [93] Vlad A, Singh N, Rolland J, Melinte S, Ajayan PM, Gohy JF (2014) Hybrid supercapacitor-battery materials for fast electrochemical charge storage. *Sci Rep* 4:4315/1–7
- [94] Roy P, Srivastava SK (2015) Nanostructured anode materials for lithium ion batteries. *J Mater Chem A* 3:2454–2484
- [95] Keppeler M, Shen N, Nageswaran S, Srinivasan M (2016) Synthesis of α -Fe₂O₃/carbon nanocomposites as high capacity electrodes for next generation lithium ion batteries: a review. *J Mater Chem A* 4:18223–18239
- [96] Yi TF, Mei J, Zhu YR, Fang ZK (2015) Li₃Cr₇Ti₆O₂₅ as a novel negative electrode material for lithium-ion batteries. *Chem Commun* 51:14050–14053
- [97] Song H, Kim YT (2015) A Mo-doped TiNb₂O₇ anode for lithium-ion batteries with high rate capability due to charge redistribution. *Chem Commun* 51:9849–9852
- [98] Liu H, Wang GX (2014) An investigation of the morphology effect in Fe₂O₃ anodes for lithium ion batteries. *J Mater Chem A* 2:9955–9959
- [99] Li YG, Tan B, Wu YY (2008) Mesoporous Co₃O₄ nanowire arrays for lithium ion batteries with high capacity and rate capability. *Nano Lett* 8:265–270
- [100] Li WY, Xu LN, Chen J (2005) Co₃O₄ nanomaterials in lithium-ion batteries and gas sensors. *Adv Funct Mater* 5:851–857
- [101] Pasero D, Reeves N, West AR (2005) Co-doped Mn₃O₄: a possible anode material for lithium batteries. *J Power Sources* 141:156–158
- [102] Wu ZS, Ren WC, Wen L, Gao LB, Zhao JP, Chen ZP, Zhou GM, Li F, Cheng HM (2010) Graphene anchored with Co₃O₄ nanoparticles as anode of lithium ion batteries with enhanced reversible capacity and cyclic performance. *ACS Nano* 4:3187–3194
- [103] Yao WL, Wang JL, Yang J, Du GD (2008) Novel carbon nanofiber-cobalt oxide composites for lithium storage with large capacity and high reversibility. *J Power Sources* 176:369–372
- [104] Yao WL, Yang J, Wang JL, Tao L (2008) A synthesis and electrochemical performance of carbon nanofiber-cobalt oxide composites. *Electrochim Acta* 53:7326–7330
- [105] Wang B, Wu XL, Shu CY, Guo YG, Wang CR (2010) Synthesis of CuO/graphene nanocomposite as a high-performance anode material for lithium-ion batteries. *J Mater Chem* 20:10661–10664
- [106] Luo YS, Luo JS, Jiang J, Zhou WW, Yang HP, Qi XY, Zhang H, Fan HJ, Yu DYW, Li CM, Yu T (2012) Seed-assisted synthesis of highly ordered TiO₂@ α -Fe₂O₃ core/shell arrays on carbon textiles for lithium-ion battery applications. *Energy Environ Sci* 5:6559–6566
- [107] Zhou WW, Chen CW, Liu JP, Tay YY, Jiang J, Jia XY, Zhang JX, Gong H, Hng HH, Yu T, Fan HJ (2011) Epitaxial growth of branched α -Fe₂O₃/SnO₂ nano-heterostructures with improved lithium-ion battery performance. *Adv Funct Mater* 21:2439–2445
- [108] Zeng WQ, Zheng FP, Li RZ, Zhan Y, Li YY, Liu JP (2012) Template synthesis of SnO₂/ α -Fe₂O₃ nanotube array for 3D lithium ion battery anode with large areal capacity. *Nanoscale* 4:2760–2765
- [109] Mondal S, Rana U, Malik S (2015) Graphene quantum dot-doped polyaniline nanofiber as high performance supercapacitor electrode materials. *Chem Commun* 51:12365–12368

- [110] Simon P, Gogotsi Y (2008) Materials for electrochemical capacitors. *Nat Mater* 7:845–854
- [111] Zhu SJ, Jia JQ, Wang T, Zhao D, Yang J, Dong F, Shang ZG, Zhang YX (2015) Rational design of octahedron and nanowire $\text{CeO}_2/\text{MnO}_2$ core-shell heterostructures with outstanding rate capability for asymmetric supercapacitors. *Chem Commun* 51:14840–14843
- [112] Spahr ME, Bitterli PS, Nesper R, Haas O, Novak P (1999) Vanadium oxide nanotubes. A new nanostructured redox-active material for the electrochemical insertion of lithium. *J Electrochem Soc* 146:2780–2783
- [113] Jiang H, Zhao T, Ma J, Yan CY, Li CZ (2011) Ultrafine manganese dioxide nanowire network for high-performance supercapacitors. *Chem Commun* 47:1264–1266
- [114] Chou SL, Wang JZ, Chew SY, Liu HK, Dou SX (2008) Electrodeposition of MnO_2 nanowires on carbon nanotube paper as free-standing, flexible electrode for supercapacitors. *Electrochem Commun* 10:1724–1727
- [115] Dubal DP, Gund GS, Holze R, Jadhav HS, Lokhande CD, Park CJ (2013) Surfactant-assisted morphological tuning of hierarchical CuO thin films electrochemical supercapacitors. *Dalton Trans* 42:6459–6467
- [116] Dubal DP, Gund GS, Holze R, Lokhande CD (2013) Mild chemical strategy to grow micro-roses and micro-woolen like arranged CuO nanosheets for high performance supercapacitors. *J Power Sources* 242:687–698
- [117] Dubal DP, Gund GS, Holze R, Lokhande CD (2014) Enhancement in supercapacitive properties of CuO thin films due to the surfactant mediated morphological modulation. *J Electroanal Chem* 712:40–46
- [118] Nwanya AC, Obi D, Ozoemena KI, Osuji RU, Awada C, Ruediger A, Maaza M, Rosei F, Ezema FI (2016) Facile synthesis of nanosheet-like CuO film and its potential application as a high-performance pseudocapacitor electrode. *Electrochim Acta* 198:220–230
- [119] Lang XY, Hirata A, Fujita T, Chen MW (2011) Nanoporous metal/oxide hybrid electrodes for electrochemical supercapacitors. *Nat Nanotechnol* 6:232–236
- [120] Sun P, Yi H, Peng TQ, Jing YT, Wang RJ, Wang HW, Wang XF (2017) Ultrathin MnO_2 nanoflakes deposited on carbon nanotube networks for symmetrical supercapacitors with enhanced performance. *J Power Sources* 341:27–35
- [121] Fujishima A, Honda K (1972) Electrochemical photolysis of water at a semiconductor electrode. *Nature* 238:37–38
- [122] Carey JH, Lawrence J, Tosine HM (1976) Photodechlorination of PCB's in the presence of titanium dioxide in aqueous suspensions. *Bull Environ Contam Toxicol* 16:697–701
- [123] Cheng S, Tsai SJ, Lee YF (1995) Photocatalytic decomposition of phenol over titanium oxide of various structures. *Catal Today* 26:87–96
- [124] Kato H, Kudo A (1998) New tantalate photocatalysts for water decomposition into H_2 and O_2 . *Chem Phys Lett* 295:487–492
- [125] Liu G, Yang HG, Pan J, Yang YQ, Lu GQ, Cheng HM (2014) Titanium dioxide crystals with tailored facets. *Chem Rev* 114:9559–9612
- [126] Sun WT, Yu Y, Pan HY, Gao XF, Chen Q, Peng LM (2008) CdS quantum dots sensitized TiO_2 nanotube-array photoelectrodes. *J Am Chem Soc* 130:1124–1125
- [127] Wang C, Wang YQ, Liu XH, Diao FY, Yuan L, Zhou GW (2014) Novel hybrid nanocomposites of polyhedral Cu_2O nanoparticles-CuO nanowires with enhanced photoactivity. *Phys Chem Chem Phys* 16:17487–17492
- [128] Diao FY, Tian FH, Liang WS, Feng HL, Wang YQ (2016) Mechanistical investigation on the self-enhanced photocatalytic activity of CuO/ Cu_2O hybrid nanostructures by density functional theory calculations. *Phys Chem Chem Phys* 18:27967–27975
- [129] Stassen I, Burtch N, Talin A, Falcaro P, Allendorf M, Ameloot R (2017) An updated roadmap for the integration of metal-organic frameworks with electronic devices and chemical sensors. *Chem Soc Rev* 46:3185–3241
- [130] Yamada T, Sadakiyo M, Shigematsu A, Kitagawa H (2016) Proton-conductive metal-organic frameworks. *Bull Chem Soc Jpn* 89:1–10
- [131] Berhe TA, Su WN, Chen CH, Pan CJ, Cheng JH, Chen HM, Tsai MC, Chen LY, Dubale AA, Hwang BJ (2016) Organometal halide perovskite solar cells: degradation and stability. *Energy Environ Sci* 9:323–356